# Ultrafast photodynamics of ZnO solar cells sensitized with the organic indoline derivative D149

by

Egmont J. Rohwer

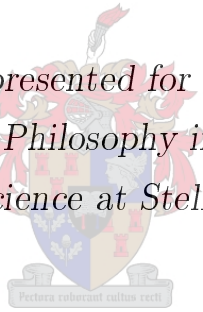

*Dissertation presented for the degree of*
*Doctor of Philosophy in Physics*
*in the Faculty of Science at Stellenbosch University*

Promoters:

| Prof Heinrich Schwoerer | Prof Derck Schlettwein |
|---|---|
| Laser Research Institute | Institut für Angewandte Physik |
| Stellenbosch University | Justus-Liebig-Universität Gießen |

April 2014

# Declaration

By submitting this dissertation electronically, I declare that the entirety of the work contained therein is my own, original work, that I am the sole author thereof (save to the extent explicitly otherwise stated), that reproduction and publication thereof by Stellenbosch University will not infringe any third party rights and that I have not previously in its entirety or in part submitted it for obtaining any qualification.

# Abstract


## Ultrafast photodynamics of ZnO solar cells sensitized with the organic indoline derivative D149

E. J. Rohwer

Dissertation: PhD Physics

March 2014

The initial charge transfer from dye molecules' excited states to the conduction band of a semiconductor, after absorption of visible light by the former, is critical to the performance of Dye sensitized Solar Cells (DSC). In a ZnO-based DSC sensitized by the organic indoline derivative D149, the dynamics associated with charge transfer are investigated with femtosecond transient absorption spectroscopy. The time-resolved measurement of the photo-initiated processes reveal electron transfer rates corresponding to excited state lifetimes of 100s of fs, consistent with previously measured high absorbed photon to current conversion efficiencies. The photo-electrode measured as an isolated system shows decay times of bound electrons in excited states of the dye to be ∼150 fs and shows the subsequent emergence of absorption bands of the oxidized molecules. When the $I^-/I_3^-$ redox couple is added to the system, these excited state lifetimes change and are found to be dependent on the cation in the electrolytic solution. Small cations like $Li^+$ reduce the excited state lifetime to sub-100 fs, whilst larger cations like the organic tetrabutylammonium result in longer lifetimes of 240 fs. The action of the electrolyte can be observed by the reduced lifetime of the oxidized dye molecules' absorption bands. The effect of operating parameters and changes in the production protocol of the DSC on the primary charge injection are also investigated and reported on.

# Uittreksel


## Hoogstydopgeloste fotodinamika van ZnO sonkragselle gekleur met die organiese indolien afgeleide D149

*("Ultrafast photodynamics of ZnO solar cells sensitized with the organic indoline derivative D149")*

E. J. Rohwer

Proefskrif: PhD Fisika

Maart 2014

Die aanvanklike ladingsoordrag vanuit kleurstofmolekules' opgewekte toestande tot in die leidingsband van 'n halfgeleier, na absorpsie van sigbare lig deur eersgenoemde, is van kritiese belang vir die uitset van halfgeleier-gebaseerde sonkragselle wat met kleurstowwe vir absorpsie verhoging, gebind is. In hierdie werk word hierdie proses en verwante fotodinamika in die geval van 'n ZnO sonkragsel gekleur met indolien D149 ondersoek d.m.v femtosekonde-tydopgelosde absorpsiespektroskopie. Hierdie metings onthul elektron-oordragstempos wat ooreenstem met lewenstye van opgewekte toestande in die orde van 100 fs. Hierdie is met voorheen-bepaalde hoë foton-tot-stroom omskakelingsdoeltreffendheid ooreenkomstig. Die foto-elektrode, as geïsoleerde sisteem beskou, toon afvalstye van gebonde elektrone in opgewekte toestande van $\sim$150 fs, en die gevolglike opkoms van absorpsie deur geoksideerde molekules word waargeneem. As die $I^-/I_3^-$ redoks oplossing tot die sisteem bygevoeg word, verander die opgewekte toestande se afvalstye en toon 'n katioon-afhanklikheid. Klein katioone soos $Li^+$ verkort die afvalstye tot onder 100 fs, terwyl groter katioone soos die organiese tetra-butielammonium langer afvalstye (240 fs) tot gevolg het. Die werking van die elektrolitiese oplossing kan waargeneem word deur die verkorte lewenstyd van die absorpsiebande wat aan die geoksideerde molekules toegeken is. Die uitwerking van operasionele parameter asook veranderinge in die produksie protokol op die primêre ladingsoordrag word ondersoek en verslag daarop word gelewer.

# Acknowledgements

My first word of thanks goes to my supervisor Prof. Heinrich Schwoerer. The guidance I have received over the years has been invaluable. His infectious enthusiasm for experimental physics creates an environment that is a pleasure to work in.

I would also like to thank Prof. Derck Schlettwein and our project partners in Giessen, Germany. In particular Christoph Richter, Kerstin Strauch and Melanie Rudolph who produced most of the samples and provided many insights during our discussions. Without these exchanges, this collaboration would not have been possible. I would also like to express my gratitude for the hospitality I enjoyed during my stay in Giessen.

Many thanks to the Stellenbosch-based students, Nadine Heming, Iulia Minda and Gabriele Tauscher who contributed over the years. I would also like to thank in particular, Drs. Christian Litwinski and Gurthwin Bosman for the mentoring role they performed during my studies. To the many students I shared laboratory and office space with as well as the rest of the students and staff at the Physics Department, my thanks for the many fond memories I will no doubt have of my time here.

My sincere gratitude to the technical and administritive staff who, on a daily basis, keep the wheels of the Physics Department's many endeavours turning.

I am grateful for the support I have received in my pursuit of further study from my family. To Néna Kotzé, I will never be able to fully express my gratitude for your love, support and understanding.

Finally I would like to acknowledge the National Research Foundation's funding of the South African Research Chair in Photonics, through which my bursary was obtained.

*meinen Eltern gewidmet*

# Contents

# Introduction

To meet future global energy demand and address contemporary concerns about the implications this may have on the environment, fingers are often pointed to the sun as a candidate for a renewable, 'green' source of energy. To date, some governments have invested heavily in the development of photovoltaic and solar thermal technologies. Vast arrays of solar panels, powered by silicon-based p-n heterojunctions have already been installed in numerous countries and laboratory efficiencies have improved to bordering on the theoretical limit. However, widespread use of this technology has been limited by high installation and maintenance costs when compared to traditional fossil fuel sources. Little reliable data is available for the expected lifetime of these panels, making investments in these products risky. This state of affairs has led to the parallel development of several alternative types of photovoltaic devices, each with the aim of finding a future in niche applications.

Dye-Sensitized Solar Cells, or DSCs in abbreviated form, is a term describing a class of photovoltaic cells that, in recent years, has generated much interest due to its potential as a future technology for harnessing the sun's radiant energy. Although the original DSC, developed by Michael Grätzel in 1991 [1], has since been optimized to deliver conversion efficiencies of up to 12% [2] and new materials and manufacturing techniques continue to improve this figure, DSCs are intended to compete for market share with conventional silicon-based photovoltaic cells on the grounds that they are cheaper to produce and more versatile for design applications.

The basic architecture of a DSC, shown in Figure 0.1, is a unit consisting of a working photo-electrode, that harvests sunlight and generates free electrons, and a counterelectrode that are connected to each other within the cell by a redox couple and externally by a circuit through which the photocurrent can flow.

Working electrodes consist partly, but primarily, of a wide-bandgap semiconductor. The semiconductor itself can generate a photocurrent, provided the incident photons match or exceed the bandgap energy and, when absorbed, excite electrons from the valence band into the conduction band. In order for the photovoltage generated by these cells to be

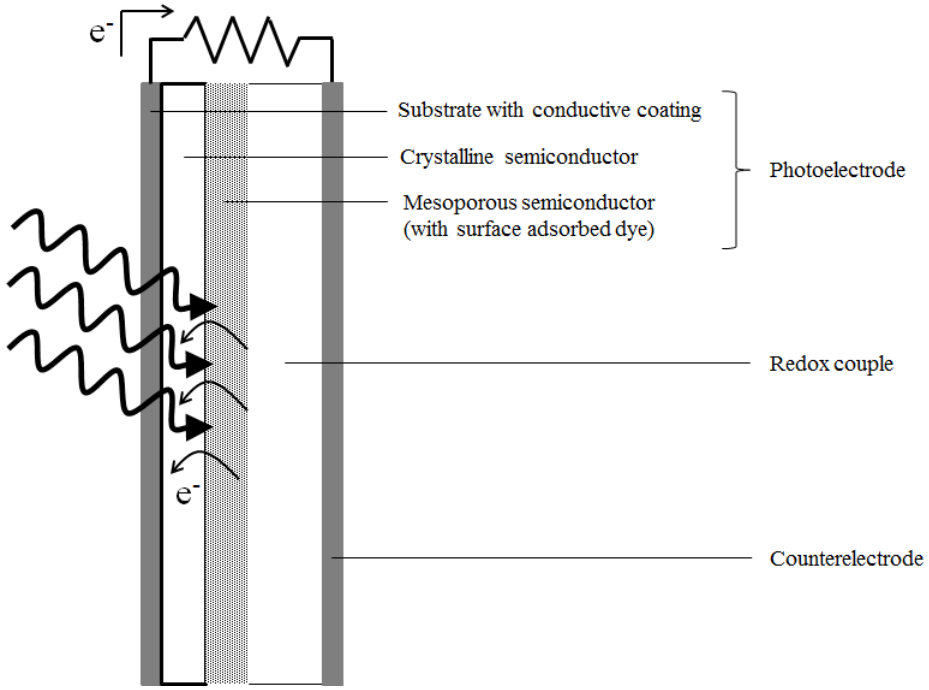


**Figure 0.1:** Schematic diagram showing a cross section of the basic DSC architecture.

in a usable regime, these semiconductors typically have bandgap energies corresponding to ultraviolet (UV) wavelengths. The sun's radiation spectrum, the source of the radiant energy that powers a solar cell, can be modelled to first approximation as the emission of a black body radiator with a surface temperature of approximately 5800 K. It therefore emits with a higher energy density both at visible wavelengths, where it peaks in the green part of the visible spectrum, and infrared wavelengths where approximately half the total solar power is found. The UV part of the solar spectrum only accounts for roughly 5% of total terrestrial radiation (see Figure 0.2). In order to sensitize the photo-electrode to longer wavelengths, a dye is attached to the semiconductor surface that absorbs in the visible or near-infrared. These molecules are chosen for their high molecular extinction coefficient and, critically, on the condition that the electron in the photo-excited state after absorption is energetically located above the conduction band edge of the semiconductor. If the coupling between the photo-excited state of the dye and the quasi-continuum of states in the conduction band of the semiconductor is sufficient, electrons can be tunnelled to the conduction band and thus enhance the solar conversion efficiency of the solar cell.

The recombination of the electron from the conduction band to the (now oxidized) dye is intercepted by the action of a redox couple. The redox couple is usually an electrolytic solution, but all-solid-state DSCs with hole conducting semiconductors [3,4] and polymers [5] have also been developed. The redox couple regenerates the neutral state of the dye by donating an electron and is itself oxidized. The oxidized state of the redox pair is in turn

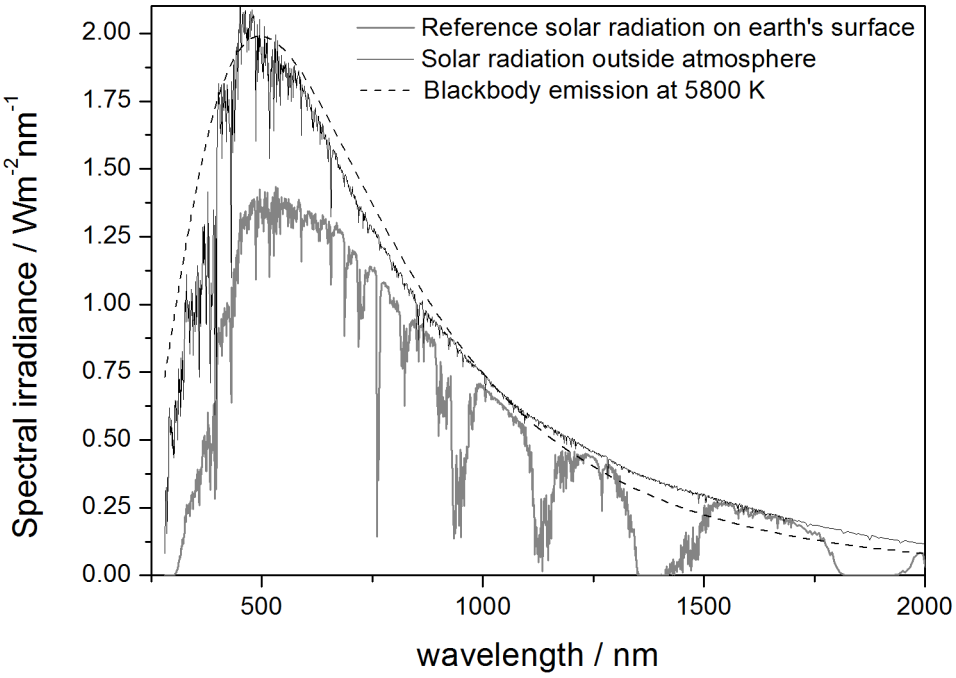


**Figure 0.2:** Solar spectral irradiance can be fitted by the emission spectrum of a blackbody radiator at 5800 K (dashed line). The dark line is the spectral irradiance at the edge of the atmosphere. The grey line represents sunlight reaching the earth's surface under clear sky conditions and at temperate latitudes. The absorption of the atmosphere is therefore taken into account. The peak emission wavelength is around 500 nm, making this a crucial spectral region to absorb sunlight in. Data for plotting of the solar radiation spectra were obtained from the website of NREL (National Renewable Energy Laboratory).

reduced by electrons at the counterelectrode. These electrons flow through an external circuit that links the electrodes, due to the electromotive force caused by the potential difference between the quasi-Fermi level of the semiconductor under illumination at the photo-electrode and the redox potential at the counterelectrode.

Many materials and combinations of materials have been used in attempts to build efficient DSCs, amongst which the only common denominator is the predominant use of a transition metal oxide as semiconducting material. An overview of some of the more successful DSCs and the materials employed will be given in a later chapter. But, at this stage it will suffice to mention that of these semiconducting transition metal oxides, ZnO has attracted attention due to several advantageous properties. Most noteworthy among them is the cost-saving implications resulting from the viability of producing photo-electrodes by electrochemical deposition. The reasons for this will be elaborated on later in this work.

Several dyes have been used with considerable success in expanding the wavelength sensitivity of a ZnO-based DSC. Of these, the indoline derivative D149 has to date shown the highest solar conversion efficiency amongst organic dyes [6]. Indoline dyes have several marketable properties, in particular and due to their organic nature; their synthesis can be adapted to customize the absorption peaks [7–9]. This implies solar cells can be manufactured with a variable colour scheme and opens up design possibilities, potentially improving consumer marketability.

The surprising efficiency achieved when dyes were successfully adsorbed to transient metal oxide surfaces and quantum efficiencies, in some cases, reported to be close to unity as determined by absorbed photon to current efficiency (APCE) measurements, resulted in interest from the ultrafast spectroscopy community. A high charge transfer rate from dye to semiconductor and consequently short lifetime of the photo-excited state of the dye in the picosecond (ps) to femtosecond (fs) regime, was inferred. This regime lent itself well to analysis by fs transient spectroscopy. The technique confirmed the high charge transfer rate by reporting charge injection lifetimes in the 100s of fs range in predominantly $TiO_2$-based samples [10–16].

At the start of my PhD, no such measurements had been published on solar cells with indoline dyes adsorbed to ZnO, despite the high efficiencies that had been achieved. It is the subject of this dissertation to report on the fs transient measurements of these samples. It will cover a condensed review of DSCs and the techniques used to characterize them, with a focus on indoline dye-sensitized ZnO cells. The technique of pump-probe spectroscopy to achieve fs time resolution and operating principles of the experimental setup used will be discussed. An understanding of the technique and how the data is recorded is critical for interpreting the transient spectra. A model for assigning spectral signatures to molecular processes will be developed as experimental data is presented stepwise in increasing system complexity from dye in solution to, eventually, its dynamics in a fully functional solar cell.

# 1. Materials and efficiency characterization of Dye-sensitized Solar Cells: a review

## *A place in the sun*

As mentioned in the Introduction, the great majority of installed photovoltaic devices are based on p- and n-doped crystalline Si. The efficiency is high, in the region of 25% [17], but so is the production cost. The remainder of the market share is divided between thin film photovoltaics which include amorphous Si, CdTe and CIGS (copper indium gallium diselenide) modules. These have reported laboratory efficiencies of 13.5%, 16.7% [18] and 19.9% [19] respectively. The relative cost saving is, however, also moderate due to the use of rare materials and expensive production equipment.

Organic photovoltaics (OPVs) is currently a growing field of research with the aim of finding cheap, abundant and environmentally-friendly materials to use in a cell with the same operating principle. The cells mentioned above consist of two layers, one electron donor and the other electron acceptor, and make use of the interface to separate electrons and holes which are transported to electrodes at opposite ends of the cell. These materials are typically bulk solid layers and as a result the language used to describe the photodynamics is borrowed from solid state physics. The layers are either p-type[1] or n-type[2] semiconductors, each responsible for transport of free electrons (n-type) and holes (p-type) in orbital bands to the anode and cathode respectively. Photons are absorbed in both layers and excitons[3] formed that diffuse to the interface of the materials where they are 'split' into free electrons and holes, sometimes assisted by the intrinsic E-field between p- and n-doped materials. These cells are still experimental and have not achieved comparable efficiencies to their inorganic counterparts [20], but long operational lifetimes are an advantage [21, 22].

Dye-sensitized solar cells are another class of alternative photovoltaic devices generating interest amongst researchers. In the language of conventional solar cells, the semiconduc-

[1] semiconductors with a Fermi level close to the valence band edge, where the majority charge carriers are holes and are thus good hole conductors

[2] semiconductors with a Fermi level close to the conduction band edge, the majority charge carriers thus being electrons rendering the material a good electron conductor

[3] bound electron-hole pairs

tor would be the n-type material and the redox couple would be the p-type, but only in the sense that the redox couple plays the role of the hole conductor. The dye monolayer that separates the two and absorbs the majority of the incoming solar radiation would be simultaneously both and neither. Since the absorption and charge separation occurs within this layer of randomly orientated, individual dye molecules where free charges are very immobile, the language of molecular physics is preferred when describing the dynamics. When photons are absorbed, excited states are populated. When charges are separated, the notion of exciton splitting is dispensed with and instead referred to as charge injection from excited states to conduction band via orbital coupling. These DSCs are designed to compete primarily on cost of production and niche application basis with other devices. Nevertheless, achieving adequate efficiency and durability is also important. In the following sections, the motivations for these assertions will be discussed.

## 1.1 DSC materials

Let's begin by reviewing the operating principle of DSCs as described in the Introduction in more detail. The processes mentioned describe an ideal scenario where every incident photon generates a free electron that is harvested at the photo-electrode and flows in an external circuit due to a potential difference generated by the incident light. In a 100% efficient cell the processes of absorption by the dye, electron injection from the photo-excited state of the dye into the conduction band of the semiconductor, diffusion of the electron through the semiconductor to the photo-electrode (anode), reduction of the oxidized dye by a redox couple and, in turn, reduction of the oxidized redox couple at the counterelectrode (cathode) happen with a quantum efficiency of unity. These 'desired' processes are labelled with arrows in Figure 1.1 numbered 1-5. Competing processes, however, limit the efficiency of DSCs. These are indicated by the arrows numbered 6 and 7 and include geminate recombination of the dye (LUMO[4]-HOMO[5] transition) and non-geminate recombination of injected electrons into the vacant ground state (HOMO) of a dye molecule. This cycle is also ideally repeatable *ad infinitum*. Indeed, electrical power is generated without permanent chemical transformation of the dye, but in practice a limited number of turnovers are possible depending largely on the dye's photo- and chemical stability.

Recently the group of Michael Grätzel at the EPFL in Lausanne, Switzerland reported a 15% external power conversion efficiency[6] for a dye-sensitized solar cell consisting of a

[4]Lowest Unoccupied Molecular Orbital

[5]Highest Occupied Molecular Orbital

[6]In this work often denoted by $\eta$, this is the proportion of total electrical power generated by the cell to the radiant energy incident on its light harvesting surface.

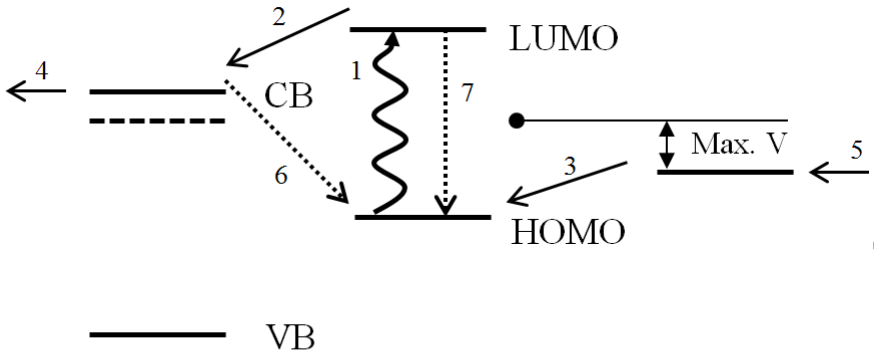


**Figure 1.1:** Simple energy level diagram of relevant internal DSC processes. The solid horizontal lines indicate electronic states in the dye, semiconductor and redox couple. The HOMO and LUMO states of the dye are labelled as such, the redox potential of the mediator is indicated and the conduction band- and valence band edge of the semiconductor are labelled CB and VB respectively. The dotted line indicates the quasi-Fermi level of the semiconductor under illumination. The difference between this and the redox potential determines the photovoltage of the cell. Processes are indicated by arrows and are numbered. Photo-excitation (1), charge injection (2), regeneration of the neutral dye molecule by oxidation of redox couple (3), electron transport to anode (4) and reduction of the redox couple by the cathode (5) represent the desired path a photo-excited electron would follow and are represented by solid arrows. Dotted arrows indicate parasitic processes that limit efficiency, electron-hole (geminate) recombination of the dye itself is numbered 7 while recombination of injected electrons (non-geminate) can also occur (6).

mesoporous $TiO_2$ electrode sensitized with perovskites [23]. Although encouraging, record efficiencies for DSCs lingered for many years around the 10% mark and during this time the motivation behind developing DSCs for eventual commercialization was that they would compete with conventional solar technologies not on a kW/cm$^2$ criteria, but rather on the basis of kW/$.

In 1991, the same man, Michael Grätzel, along with Brian O'Regan reported in their seminal paper that efficiencies of 7.1-7.9% in direct sunlight had been achieved using a 'colloidal $TiO_2$ thin film' and ruthenium-based dye [1] (although this was not mentioned in the paper and referred to as a charge transfer dye). Before, DSC efficiencies remained below even 1% and this work precipitated a dramatic increase in research output on the topic of DSCs. The crucial insight resulting from the research was that the materials used need not be smooth or highly crystalline, as was the belief with the more established silicon solar cells. The almost order-of-magnitude increase in efficiency was attributed to the highly structured, porous surface morphology of the $TiO_2$ that allowed for higher dye-sensitization due to the increased surface area. Research had shown that in order for

electron injection to take place, excited state orbitals in the dye need to overlap with the conduction band of the semiconductor [24]. Oxidized dye molecules also need to be in contact with an electrolyte in order to be regenerated. Since excitons diffuse poorly in these adsorbed dye networks, meeting the criteria listed in the previous sentences is only feasible if a monolayer of the dye is deposited. Before 1991, the fundamental constraint limiting efficiency was that a monolayer of dye adsorbed to a smooth surface simply did not absorb sufficient sunlight. Attempts at multilayer cells produced no significant improvement, but with the breakthrough of Grätzel and O'Regan, the high roughness factor provided a huge surface area for sensitization. Mesoporous DSC photo-electrodes have surface areas a thousand times the dimensions of the substrate they are deposited on. An added advantage is that because of the random orientation of the porous metal oxide surface, DSCs outperform conventional silicon cells in diffuse light as is more often than not the case in colder climates. Interest in DSCs has also been stimulated due to the economic benefits that DSCs demonstrated in their ease of manufacture, with low cost and the use of abundant materials. Especially attractive is the expected low energy payback times (EPT). That is, the operational time that a photovoltaic device requires in order to generate the energy equivalent to what was used to produce it.

Since the 1991 breakthrough in the field, a variety of materials have been experimented with. Concomitantly, research output in the field of DSCs has burgeoned. Semiconductor surfaces with high roughness factors have been successfully developed with primarily transition metal oxides. These include $TiO_2$, ZnO and $Nb_2O_5$ ($SnO_2$, a post transition metal, has also been used).

Many more dyes have been utilised in conjunction with these semiconductors. Ruthenium complexes and other organometallic complexes such as porphyrins [25] and phthalocyanines [26] have shown high efficiencies. Fully organic dyes have also been employed. These include coumarins [27], styryls [28] and indoline dyes [6, 29].

Electrolytes have been varied greatly in research conducted on DSCs. So numerous are the materials and compositions experimented with that for the sake of brevity I will simply list the categories they can be arranged into; solid organic- and inorganic hole conductors, gel and polymer electrolytes, ionic liquids and redox couples in solution [18]. Solid inorganic and organic hole conductors have attracted interest because they are believed to be more robust, do not leak and cells can be transported with ease. Typically these hole conductors (as well as gels and polymers) have failed to achieve desired efficiencies due to their high viscosity during the manufacturing phase. They are thus unable to fill the finer pores on the dye-coated semiconductor surface and as a result provide poor contact at the semiconductor/dye/electrolyte interface. It should be noted, however, that a recent paper reported that an all-solid-state DSC had achieved efficiencies of 10.2% [3]. Despite this

the most popular and still best performing regenerating phase remains the electrolyte used in the Grätzel cell of 1991, the iodide/tri-iodide ($I^-/I_3^-$) redox couple. Variations in composition have not significantly improved performance, however the cations used in solution have been found to affect the open circuit voltage. This will be elaborated on later. The use of the $I^-/I_3^-$ redox couple does have an important drawback; it is known to be chemically volatile and corrosive, properties that affect the long term performance and lifetime of cells.

At the forefront of advances in efficiency since 1991 have generally been DSCs consisting of mesoporous $TiO_2$, a ruthenuim complex as a dye (the N3, N719 and N749 complexes have been most successful [2, 30]) and an iodide/tri-iodide liquid redox couple as electrolyte. As a result, extensive research and characterization has been done on these samples and will be referred to for comparison in this work. Since DSCs are meant to compete in the photovoltaic market on economic grounds, it is equivalent to pursue cells that can be produced as cheaply as possible with reasonable yield as to pursue efficiency at a reasonable price. In this context, a DSC employing a porous ZnO as semiconductor, an indoline dye as sensitizer and iodide/tri-iodide electrolyte becomes a promising candidate. ZnO is an apt replacement for $TiO_2$; it has a similar bandgap and higher carrier mobility [31, 32]. Where ZnO really outperforms $TiO_2$, the difference can be measured in dollars and cents. The production of a mesoporous network of $TiO_2$ requires sintering at a temperature of 450°C. Colloidal thin films of $TiO_2$ nanoparticles are electrically contacted in this way. Production of a porous ZnO can be done by electrochemical deposition that occurs optimally at 70°C. This implies not only a lower EPT but also that substrates do not need to withstand 450°C. Cheap, flexible plastic substrates can thus be used instead of glass. The indoline derivative D149 has to date, among organic dyes, provided the highest overall efficiency (5,56% [29]). Organic dyes are easily synthesized and made from abundant materials and comply with the present economic considerations. The plastic substrates and the relative ease with which organic molecules can be tuned to absorb at different wavelengths, means that the ZnO-indoline dye combination can be customized for colour, application, surface geometry and substrate.

## 1.2 Characterization of DSCs

Several techniques are routinely used to characterize and compare the performance of DSCs and understand their operation at various levels. In this section, the standard performance characterization techniques will be briefly reviewed.

In order to compare solar cells' photon-to-current conversion performance, a standardized source of radiant energy is required. Since the solar flux at any laboratory or testing

facility depends heavily on geographic location, time of day, season and atmospheric conditions, solar simulators are utilised. They are intended to produce an ideal AM 1.5 G irradiance spectrum, although in most cases corrections need to be made. The AM 1.5 G[7] irradiance spectrum is the solar radiation spectrum expected on a clear day with the sun at an angle of elevation of 42°, which is then normalized to provide an intensity of 1000 $W/m^2$ (see light grey line in Figure 0.2). This light source illuminates the DSC which is coupled to an external circuit with a variable bias potential. To determine the power conversion efficiency, a current-voltage (I-V) curve is recorded. This graph is populated with measurements of the current produced by the DSC, under illumination, as a function of the applied bias potential. An example of such a graph is shown in Figure 2.2. The maximum power conversion efficiency is achieved at the point where the product of V and I is a maximum and can be calculated as the ratio of the product of the current and voltage at this point to the power of the incident light. Other parameters that can be determined from an I-V curve and are in common parlance in the DSC field, and indeed photovoltaics in general, are the short circuit current density ($J_{SC}$) and the open circuit voltage ($V_{OC}$). The $J_{SC}$ is the current density when no bias potential is applied (intercept on the ordinate axis) and the $V_{OC}$ is the bias potential value when the current stops flowing (intercept on the abscissa) as is the case when the electrodes are not contacted, therefore 'open circuit'. The fill factor is a value between 0 and 1 that describes how well the area under the I-V curve covers the area of the rectangle with opposite corners at $J_{SC}$ and $V_{OC}$. A lower fill factor generally implies more power is dissipated in internal resistances, leak currents and recombination events. The aforementioned parameters are related mathematically in Equation 1.1,

$$\eta = \frac{J_{SC} V_{OC} FF}{P_{in}}, \tag{1.1}$$

where $\eta$ is the overall cell efficiency, FF is the fill factor and $P_{in}$ is the incident radiative power. Incident photon to current conversion efficiency (IPCE) measurements determine the response of DSCs to monochromatic light. An IPCE spectrum plots the efficiency as a function of wavelength and therefore in most cases resembles the absorption spectrum of the sensitizer. IPCE spectra for ZnO/D149 DSCs can be seen in Figure 2.3. Overall efficiency can be calculated from a cell's IPCE spectrum. The IPCE, LHE[8], $J_{SC}$ and overall efficiency are related by the following set of equations,

$$\eta = \frac{\int P_{in}(\lambda) IPCE(\lambda) d\lambda}{\int P_{in}(\lambda) d\lambda}, \tag{1.2}$$

[7] AM stands for air mass and G stands for global with 1.5 being a measure of atmospheric path length
[8] Light Harvesting Efficiency

$$IPCE(\lambda) = \frac{J_{SC}}{eI_0(\lambda)} = LHE(\lambda)\eta_{inj}(\lambda)\eta_{cc}(\lambda), \tag{1.3}$$

where e is the elementary charge, $I_0$ is the photon flux density, LHE is the Light Harvesting Efficiency and $\eta_{inj}(\lambda)$ and $\eta_{cc}(\lambda)$ are the quantum efficiencies of electron injection and charge collection respectively. From the equations it is evident that $\eta$ is a measure of the ratio of the *total* electron flux density to the *total* photon flux density where IPCE is a measure of the same ratio as a function of wavelength. Usually IPCE spectra are measured under short circuit conditions. Absorbed photon to current efficiency (APCE) is sometimes mentioned in Literature and can be calculated from IPCE spectra. The APCE assumes that photons have been absorbed and is an indication of the quantum efficiency of subsequent processes following photo-excitation of the dye. The mathematical relation is given in Equation 1.4.

$$APCE(\lambda) = \frac{IPCE(\lambda)}{LHE(\lambda)} = \eta_{inj}(\lambda)\eta_{cc}(\lambda). \tag{1.4}$$

APCE provides insight on the combined efficiency of electron injection, charge transport and dye regeneration. Ultimately, how likely is the outcome that an electron bound in the excited state of a dye following absorption will end up as a free electron in the external circuit? In successful DSCs these probabilities are high, in the region of 80% and upwards, indicating that electron injection is a very favourable deactivation mechanism of the dye's excited state. We will revisit this topic later, but it explains why much of the research conducted today is aimed at extending the LHE.

From these measurements of the macroscopic properties of the cells, some estimation of the microscopic dynamics can be inferred. But to obtain quantitative data, a more sensitive approach is required. One such technique is femtosecond transient absorption spectroscopy (fs-TAS), where it is possible to directly measure reaction rates of molecular processes. The data obtained from these measurements can help to optimise the operation of the DSC at a molecular level. In the following chapters fs-TAS as an experimental technique will be introduced and the production of indoline sensitized ZnO DSCs and characterization by other techniques will be covered. We will begin with the latter.

# 2. Sample preparation and characterization

In this chapter the process by which a fully functional D149/ZnO DSC is produced by our project partners in Giessen, will be outlined. Subtle changes in the production protocol are made and the potential effects investigated with fs-TAS measurements, which is the subject of the results chapter. But before these effects are investigated it is necessary to understand where they may originate, which is the business of the first part of this chapter. How and why certain materials and production techniques are employed will be explained.

The second part of this chapter will discuss what has been learnt about DSC's (D149/ZnO and other combinations) by others using a variety of experimental techniques in Literature. This will shed light on the benefits and drawbacks of certain materials and how they are expected to enhance or limit cell performance. Once the necessary background information has been established, the fs-TAS results are used to comment on the cell performance outcomes, predicted or otherwise, in the results chapter.

## 2.1 Production of indoline D149-sensitized ZnO solar cell

This section is divided for ease of reference into 3 sub-sections, each discussing the sample preparation in 3 basic steps namely: deposition of the semiconductor, sensitization with the dye and cell fabrication. This technique was developed by our project collaborators in Giessen, Germany. Although many of the samples measured during my PhD (specifically the first generation photo-electrodes) were made by me, under knowledgeable supervision, during my research visit to the laboratories in Giessen, fully functional DSCs that were subsequently investigated, were produced by our collaborators. I am indebted to them for their efforts.

### Porous ZnO structure by electrodeposition

For robustness and optimal optical transmissivity the substrate for the cell architecture is glass. One side of the substrate is covered with a conductive Fluorine-doped Tin Oxide (FTO) layer (Asahi Glass 12 $\Omega/\square$). The plates are stored in isopropanol and when

removed, dried with $N_2$ gas. In order to activate the surface for electrodeposition, the plates are submerged in nitric acid for 2 minutes and subsequently rinsed with deionized water and dried with $N_2$ gas once more. Electrodeposition occurs in a home-built setup. The glass plates are placed on a sample mount attached to a rotating disc electrode. Electrical contacting of the FTO layer is achieved with copper tape. Insulating tape is then cut to cover all but the surface of the glass plate intended for ZnO deposition. This surface is typically 1.5 x 1.5 cm and exposed by submersion in a beaker to a 0.1 M KCl solution. For optimal deposition in terms of structure porosity, reaction rate and macroscopic homogeneity of the surface thickness, the sample holder is rotated at 500 rpm and the aqueous KCL solution heated to 70°C and saturated with bubbling oxygen gas at 400 mL/min. The ZnO phase, as suggested before, is deposited by electrochemical means in a three electrode setup. The working electrode consists of the electrically contacted-, FTO covered glass plate itself. A Zn wire forms the counterelectrode and the applied potential is monitored by a commercial reference electrode (Radiometer Analytical, 0 mV vs Ag/AgCl).

The actual deposition occurs in 3 stages. A potential of -1060 mV (vs Ag/AgCl) is applied for 30 minutes and the surface is activated. A dense crystalline layer of ZnO is deposited by adding a few drops of 5 mM $ZnCl_2$ to the solution. The deposition continues for 5 minutes and results in a layer thickness of about 500 nm. The crystalline ZnO acts as a hole-blocking layer preventing direct electrical contact between the electrolyte, sometimes referred to as the hole conductor, and the photo-electrode that harvests electrons and would otherwise result in short circuiting. In a purely porous ZnO structure the electrolyte may filter through and provide direct electrical contact between electrodes. The deposition of the porous ZnO proceeds with the addition of 50 $\mu$M of a structure-directing agent eosinY, a molecule that acts as a spacer and catalyst for the reaction. Additionally, the applied potential is lowered to -960 mV for 5 min before the deposition phase is complete. Upon removal from the electrochemical deposition setup, the exposed surface is rinsed with deionized water. The samples are then left overnight in an aqueous KOH solution of pH 10.5, during which the eosinY molecules are desorbed from the sample leaving behind vacancies in the ZnO layer deposited in the $3^{rd}$ stage and resulting in a highly porous structure. A visualization of this process is shown in Figure 2.1.

## Dye sensitization of photo-electrode

Before sensitization, samples are heated in an oven to 100°C for 1 hour to evaporate any residual water. The hot samples are then removed and submerged in an equal parts acetonitrile and *tert*-butyl alcohol solution of 0.5 mM indoline D149 (Chemicrea Co, Japan). In some cases, 1 mM cholic acid is added to the solution as co-adsorbate. It

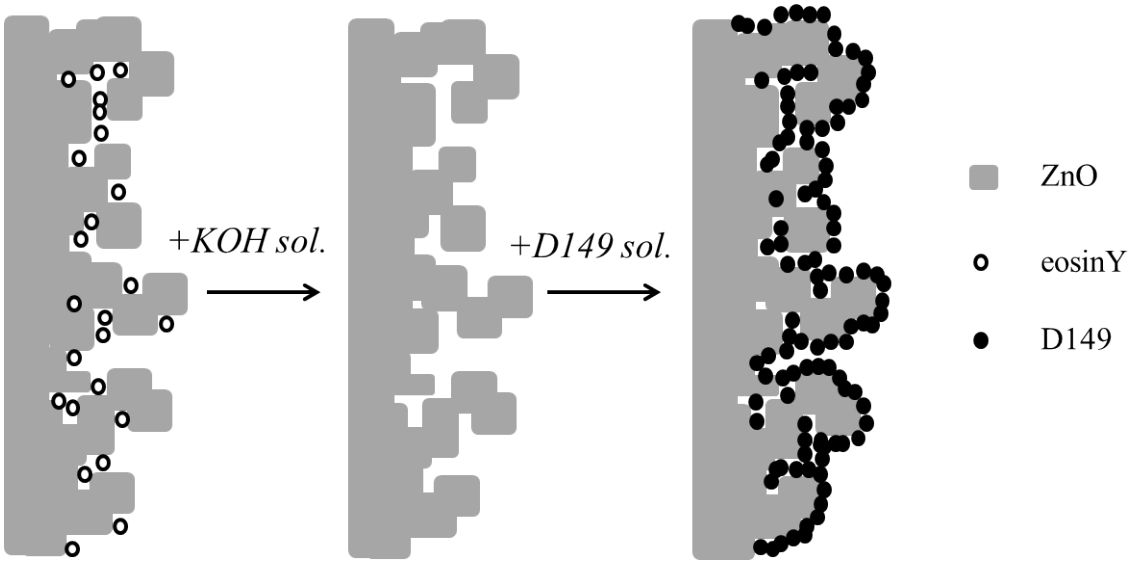


**Figure 2.1:** Illustration of dye adsorption process. The structure directing agent eosinY, represented here by empty circles, acts as a spacer during the electrochemical deposition of the porous ZnO structure (grey shape) and are removed by rinsing with an alkaline KOH (aq) solution. D149 molecules (filled circles) are adsorbed by submerging the ZnO electrode in a solution of D149 in 1:1 acetonitrile and *tert*-butyl alcohol (which includes 1 mM cholic acid in most cases).

has been shown to prevent dye-aggregation [33]. When pursuing high efficiencies, these photo-electrodes would spend 30 minutes in the solution whilst D149 molecules adsorb. This allows for optimal dye-loading of the photo-electrode surface before the detrimental effects of dye-aggregation due to overloading infringe on cell performance. However, these samples typically absorb too much light for fs-TAS measurements in transmission to be viable. The rough dispersive surface also makes an experimental configuration in reflection unsuitable. Therefore, the samples prepared for fs-TAS experiments were dye-loaded for 1 minute. The resulting dye layer was suitably transmissive across the visible spectrum so that sufficient probe white light could be transmitted and detected, but also sufficiently absorptive in order for changes due to excitation to result in a large signal. It also makes a monolayer of dye-covering all the more likely and makes the probability of detecting a signature due to charge transfer, of which practically only the surface layer can partake in, higher. The high yield of electron injection seen in the measurements reported on in the results chapter and absorption properties are consistent with this assumption. The reduced dye-loading in practice also means that recombination between the electrolyte and uncovered ZnO becomes more likely, but this occurs on a longer timescale. After removal from the dye solution, the sample is washed with ethanol to remove loosely-bound molecules and dried under a nitrogen stream.

### Cell fabrication and addition of electrolyte

The sensitized photo-electrode is placed in a sandwich configuration with the counter-electrode with a melt-sealing foil between them. The counterelectrode is simply the same conducting glass plate used as substrate in the photo-electrode. The foil (jurasol B, juraplast GmbH) seals the cell when melted at 120°C and provides electrical insulation to both electrodes from the other. The space between the electrodes, about 40 $\mu$m thick as determined by the sealing foil, can be filled with a fluid through a pre-drilled hole in the counterelectrode by vacuum backfilling. The hole is then sealed with the melt foil. The space is intended for the addition of the redox couple/hole conductor. For reasons that will become apparent in the later part of this chapter, a variety of electrolytes were added to our samples. These included tetra-butylammonium iodide (TBAI), tetra-butylammonium perchlorate ($TBAClO_4$), lithium perchlorate ($LiClO_4$) and $I_2$. The solvent in all cases was a mixture of ethylene carbonate and acetonitrile in the ratio of 4:1. For a reference experiment, one sample was filled with inert $N_2$ gas.

## 2.2 Photo-electrochemical properties

As mentioned in the opening chapter, central to the evaluation of any DSC's photochemical performance is the I-V curve. The record-holding D149/ZnO DSC was characterized in a paper by Yoshida et al in 2009 [29]. The cell was found to have a $J_{SC}$ of 12.23 mA/cm$^2$ and an $V_{OC}$ of 691 mV. The fill factor of 0.658 resulted in an overall maximum energy conversion efficiency of 5.56%. The I-V curve of a cell manufactured by our collaborators with optimized dye-loading is shown in Figure 2.2 and compares well with the specifications above.

The IPCE spectra (Figure 2.3) showed values above 80% in broad regions around the absorption band maxima at 527 nm and 380 nm and generally above 60% from the bandgap absorption edge of ZnO to 600 nm[1]. Considering that an estimated 10% of incident light is lost by reflection off the front and FTO-covered back surface of the photo-electrode's glass substrate, the internal photon-to-current quantum efficiency at the absorption maxima approaches 100%. For surface adsorbed excited dye molecules, the electron injection mechanism should then have a high rate to compete with other processes and achieve such a yield. This is thus the first indicator of an ultrafast process.

Much mention has been made of the lamentable corrosive effects of the $I^-/I_3^-$ redox couple in solution and for this reason attempts at solid state or gel redox couples have been made, unfortunately without comparable efficiency. The principle reason why developers of

[1]For DSCs with optimal loading. The samples measured with fs-TAS (1-2 min dye loading) show maximum IPCE of about 60%.

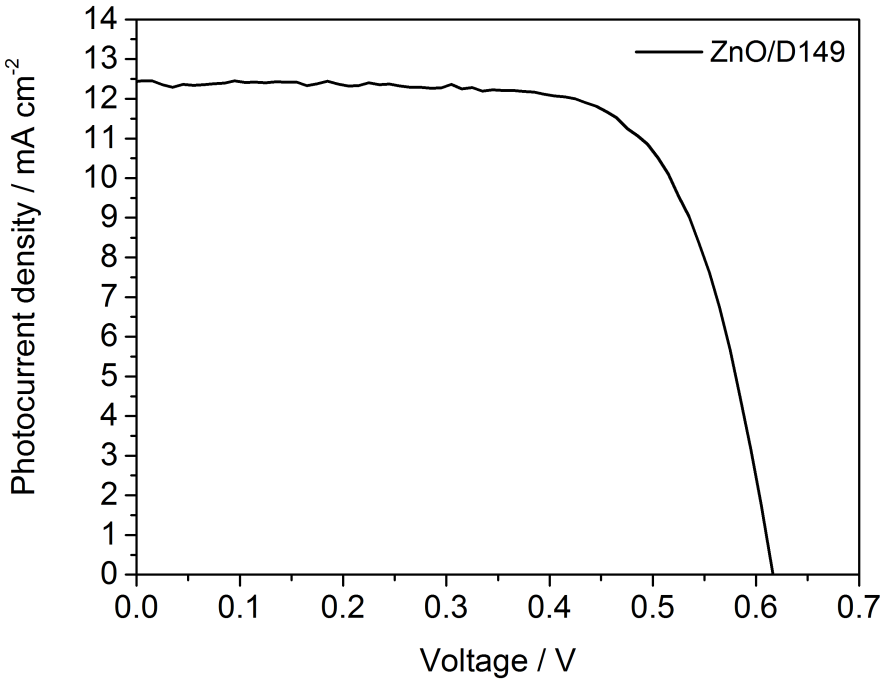


**Figure 2.2:** I-V curve of the D149/ZnO as manufactured for our fs-TAS experiments, but with optimized dye-loading for maximum efficiency. The $V_{OC}$ can be read off the intercept on the horizontal axis. The intercept on the vertical axis is the $J_{SC}$.

DSCs persist with the use of $I^-/I_3^-$ is because the oxidation rate of iodide is quick while the reverse reaction (reduction of tri-iodide) is relatively slow as iodine-iodine bond-breaking is involved. This means that oxidized dye molecules by electron injection to ZnO can be rapidly reduced by the oxidation of iodide but, more importantly, that recombination of the reduced neutral dye molecules with the oxidized species tri-iodide is inhibited.

A paper by Wang et al in 2012 [34] studied the effect of the cation used in electrolytes containing the $I^-/I_3^-$ redox couple. They compared 4 cations namely; the organic $TBA^+$ (tetra-butylammonium), $Li^+$, $Na^+$ and $Mg^{2+}$ and found trends related to the charge/radius ratio of the cations to their respective I-V curves. They found, for example, that the $V_{OC}$ was inversely proportional to the charge/radius ratio, effectively charge density, of the cation. They also found that the $J_{SC}$ was similar for $Na^+$, $Li^+$ and $Mg^{+2}$ but significantly less for the much larger $TBA^+$. The IPCE values were also consistent with the $J_{SC}$ trend. However, the spectral position of the dye's[2] absorption features did not shift as the cation was changed, indicating that the HOMO-LUMO gap was unaffected. Since the same redox potential applies for all cells, corresponding to that of the $I^-/I_3^-$ redox couple, the change in $V_{OC}$ was interpreted as a shift in the conduction band edge of the semiconductor[3] and thus the quasi-Fermi level. It was predicted that the lowered conduction band edge

[2] in this case the ruthenium complex N719
[3] in this case $TiO_2$

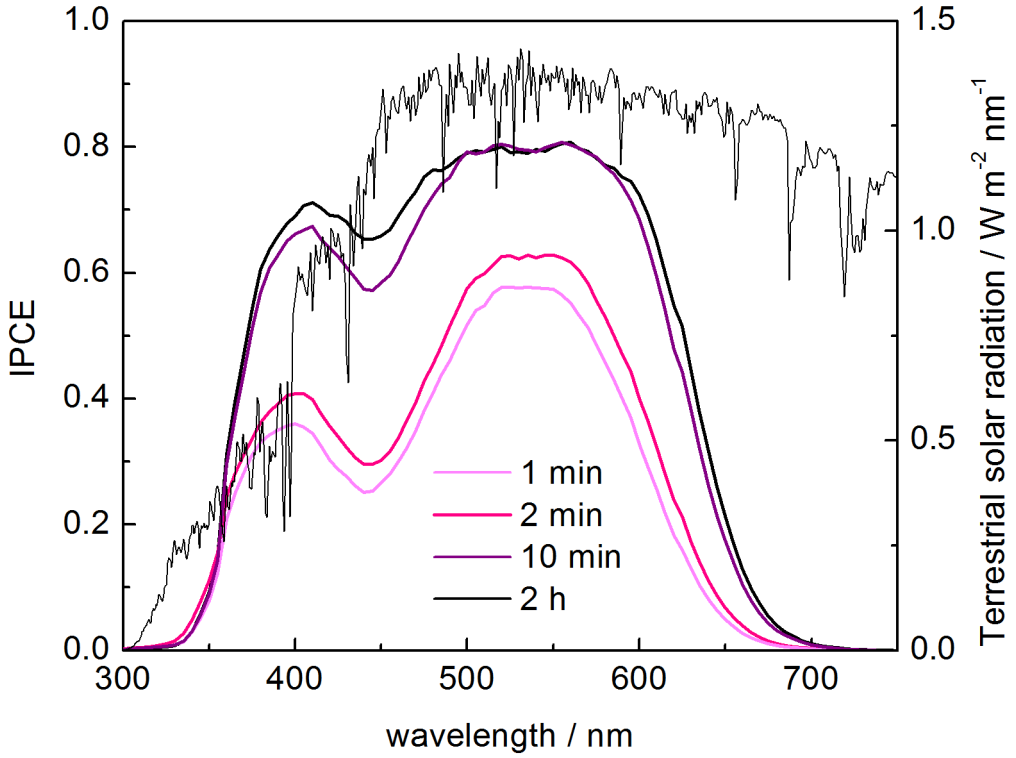


**Figure 2.3:** Wavelength dependent Incident Photon to Current conversion Efficiencies (IPCE) of ZnO/D149 DSCs with different dye-loading. The AM 1.5 G standard solar radiation spectrum is plotted as reference.

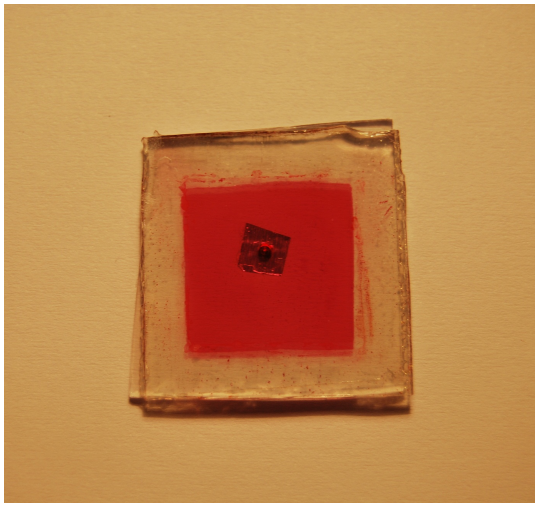

**Figure 2.4:** Image of complete D149/ZnO DSC. The aluminium foil sealing the pre-drilled hole through which the electrolyte is filled, can be seen. The active area of the cell is 1.5 cm x 1.5 cm, to the naked eye it has a pinkish colour and this particular sample shows remarkable homogeneity across the deposition surface.

caused an improved overlap between the density of states in the conduction band and the LUMO of the dye. This would infer a faster electron injection rate and account for the improved IPCE and $J_{SC}$ values. This effect has since been directly observed by transient absorption spectroscopy for $TiO_2$ based DSCs with coumarin [16]- and ruthenium [35] based dyes, but remains to be witnessed for the D149/ZnO DSC.

The tendency for D149 molecules to aggregate is a concern for developers of indoline-sensitized solar cells. A paper by Sakuragi et al in 2010 [33] studied the effects of aggregation on D149/ZnO DSCs. Cells produced with and without co-adsorbing cholic acid, a co-adsorbate in the dye adsorption process that prevents aggregation, were subjected to photo-electrochemical characterization. The resulting I-V curves showed a more rounded curve indicating a poor fill factor for cells without cholic acid that are more susceptible to aggregation. The same study investigated the effects of dye-loading on the cell. Although cells, that were soaked in the dye solution longer, showed broader and larger amplitude absorption bands due to aggregated molecules and thus higher LHE, the IPCE values reached an optimal value at an intermediate soaking time before deteriorating with further dye-loading. IPCE and LHE are related by Equation 1.3. Since the charge collection efficiency can be assumed to be the same for all samples because the same ZnO electrode and electrolyte is used, the deterioration of the IPCE with increased dye-loading past an optimum is assigned to a reduction in charge injection efficiency. The fill factor for each cell, however, was consistently better for cells with less dye-loading. This observation implies that dye aggregation may lie at the heart of the deteriorating charge injection efficiency. The paper attributed the poor fill factors and charge injection efficiency to aggregate formation that resulted in deep trap sites for recombination. Adding a co-adsorbate to the cell consistently offset the negative effects of excessive dye-loading, improving IPCE and fill factors when comparing cells with the same soaking time but without co-adsorbate. The co-adsorbate is therefore believed to suppress aggregate formation. Another study by El-Zohry et al [36] showed that aggregate formation in D149/$TiO_2$ DSCs showed reduced fluorescence lifetimes and may have consequences on electron injection efficiency since faster competing deactivation mechanisms arise. Despite the parasitic effects of aggregation, the addition of co-adsorbate does mean ZnO surface sites are occupied by co-adsorbate. While these do separate D149 molecules and prevent unnecessary deactivation and recombination, they also occupy sites that could have been covered with dye and extended the LHE. It is our hope that fs-TAS will shed light[4] on these effects especially on the fastest of processes, the electron injection from dye to semiconductor.

[4] if you will excuse the pun

# 3. Transient Absorption Spectroscopy with fs resolution: the pump-probe technique

In order to interpret the data presented in the results chapter, a thorough understanding of the experimental technique is required. This chapter, as the title suggests, will explain how the high temporal resolution required to measure the fastest dynamics expected in a DSC is achieved. The technical specifications that enable these measurements will be discussed along with their limitations. The specifications of the setup used to obtain the data presented in this dissertation will be disclosed. The collection, processing and graphical representation of the experimental data will be explained.

## 3.1 Achieving fs resolution

You can't measure a molecule with a yardstick[1]. In order to measure the photodynamics of the dye in a DSC, which could be in the fs regime, we require a probe of a comparable magnitude and equal dimension.

Commercially available fs laser sources producing optical pulses of fs duration provide just such a measuring tool. In order to determine any duration a 'start' needs to be defined with sufficient accuracy. Since the energy conversion process in DSCs is photo-initiated, an incident optical pulse can be used as a trigger that defines the start of the process with a certainty within its duration. Similarly, these pulses can also be used to probe the state of a sample. As in steady state absorption spectroscopy, light can probe the population distribution of states in an ensemble of molecules by measuring its absorption spectrum. Should this light be pulsed, the properties of this measuring tool allow that the population of states can be determined under non-equilibrium conditions at a specific time with a precision within the pulse duration, provided the sample interacts with the wavelengths within the pulse's bandwidth spectrum. The temporal resolution of such an experiment would be determined by the cross-correlation of the pulse that triggers the process and the pulse that probes the state of the evolving photo-initiated process. If you have a fs laser source, you have resolution in the fs regime. However, there is no electronic detector that can record data with a petahertz repetition rate (1 fs period $\hat{=}$ 1

[1]Nor is it sensible to measure, for argument's sake, national borders with the same yardstick.

PHz frequency). Electronic circuitry can simply not be made small enough. To overcome this limitation and make use of a slow detector, the pump-probe technique is employed.

Allow me to conceptualize the pump-probe technique with the aid of a metaphor. Imagine you are tasked with making a video of an athlete running a race, but the only instrument at your disposal is a conventional still photo camera. The shutter speed is fast enough to capture a still frame of the athlete's stance sufficiently resolved at any time, but the camera needs a few seconds to charge the capacitors for the flash and move a new section of film into position for the next exposure to be taken. Its frame rate is thus insufficient to capture successive still frames that can describe the motion.

This scenario can be likened to the one outlined in the previous paragraph. Some analogies can be made; the trigger for this sprint is the starter's pistol (which also needs to be sufficiently short in duration). The shutter speed determines the exposure of the film to ambient light and results in a still photograph in this case. Critically it is not the development of the photograph, which is slow, that determines the temporal sensitivity of the probe, but rather the shutter speed. We therefore regard the shutter mechanism as the probe and the film as the detector.

It is impossible for a recording of the dynamics to be taken in one race. This problem can be bypassed if more than one race is run. Instead of attempting to photograph the athlete at multiple times during one race, we photograph the athlete once during multiple races at different times after the start. If we take a photo a fraction of a second after the starter pistol has been fired in the first race and then take a photo at multiples of that fraction of a second after the start in successive iterations of the race, the still frames could be spliced together and a film of the race can be made. This, of course, rests on the assumption that the athlete is in the same condition before each race and that the athlete runs an identical race each time. It is perhaps unrealistic to expect a single athlete to run an identical race $n$ times, but when considering a statistical ensemble of molecules the average dynamics are, for all practical purposes, identical.[2]

Probing sub-picosecond (ps) scale dynamics in scientific samples is enabled by the pump-probe technique. The sample is illuminated with an optical pulse with a wavelength tuned to an absorption band of the sample. Absorption by the sample populates excited states. This pulse is called the 'pump', as it deposits energy in the sample and triggers the

[2]You could argue that one could also use multiple cameras, each taking a still photo at different times during one race but this doesn't translate well to the DSC scenario. Besides being potentially costly (multiple spectrometers and laser sources), a PHz repetition rate laser would be likely to cause multi-photon processes to occur and would result in a pulse train not easily separated and directed into different entrance slits of multiple slow spectrometers since one spectrometer will integrate over all pulses within the period of its readout rate. Of course, the fundamental problem is that a PHz repetition rate laser does not exist. All in all it is a laughable consideration.

photo-initiated processes. The excited sample then decays by various mechanisms from excited states back to the ground state. At a specified time during this evolution the probe pulse measures the absorption of the excited non-equilibrium sample which, when compared to the ground state spectrum at equilibrium, indicates changes caused by the states in non-equilibrium. The time after excitation when the evolving system is probed is determined by the optical beampath difference between the pump and probe pulse. The pathlength difference translates to a time delay proportional to the speed of light. A data point is recorded by a detector for a fixed time after excitation. The detector can be slow, in fact the data can be averaged over many iterations of the sample excitation, determined by the detectors sampling time and the repetition rate of the laser source, improving sensitivity. A data point at another time after excitation can be recorded by changing the beampath difference. This process can be repeated for different delay times until the recorded data populates a graph with change in absorption signal on the ordinate and time on the abscissa. The recorded temporal evolution of a spectral signature can then be fitted with appropriate functions, selected based on considerations of reasonable kinetic models. The resulting decay curve is fitted to the data points and a decay time constant can be extracted.

## 3.2 The LRI setup

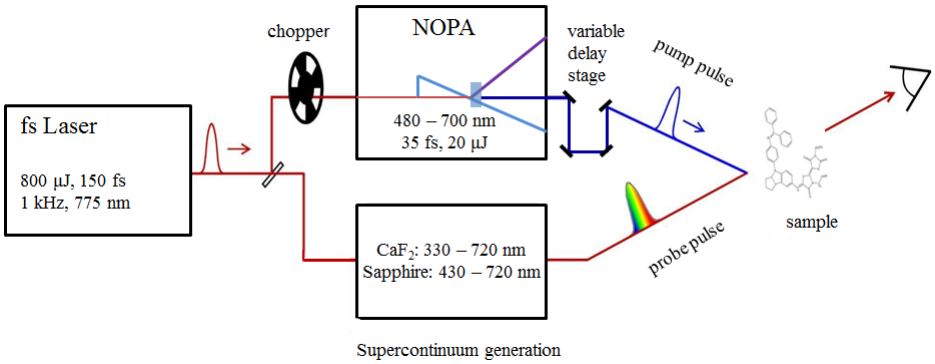


**Figure 3.1:** Schematic overview of the LRI setup.

The specifications of the LRI (Laser Research Institute) setup are summarized and layout presented in Figure 3.1. As with all fs-TAS (femtosecond Transient Absorption Spectroscopy) setups, the setup at the LRI employs the same laser source for the pump and probe pulses. The beampaths for both pulses originate at a common optical element, in this case a beam splitter. This allows for maximum phase stability between pump and probe pulses and ensures that the temporal resolution is not limited by unnecessary

temporal incoherence. At the LRI, this source is a Clark-MXR CPA[3] 2101 fs laser. It is an Yb-doped fibre laser producing 150 fs laser pulses at 1550 nm. The pulse energies are boosted in a regenerative Ti:Sapphire amplifier. The system produces polarized 150 fs pulses at 775 nm with about 800$\mu$J pulse energies at a 1 kHz repetition rate. About 30% of the pulse energy is directed, by choice of appropriate beam splitters, to a non-colinearly phase-matched optical parametric amplifier (NOPA). The NOPA allows for a tunable output between 480 and 700 nm by parametric amplification of sapphire-generated white light in a beta-barium borate (BBO) crystal pumped by the frequency doubled CPA output.

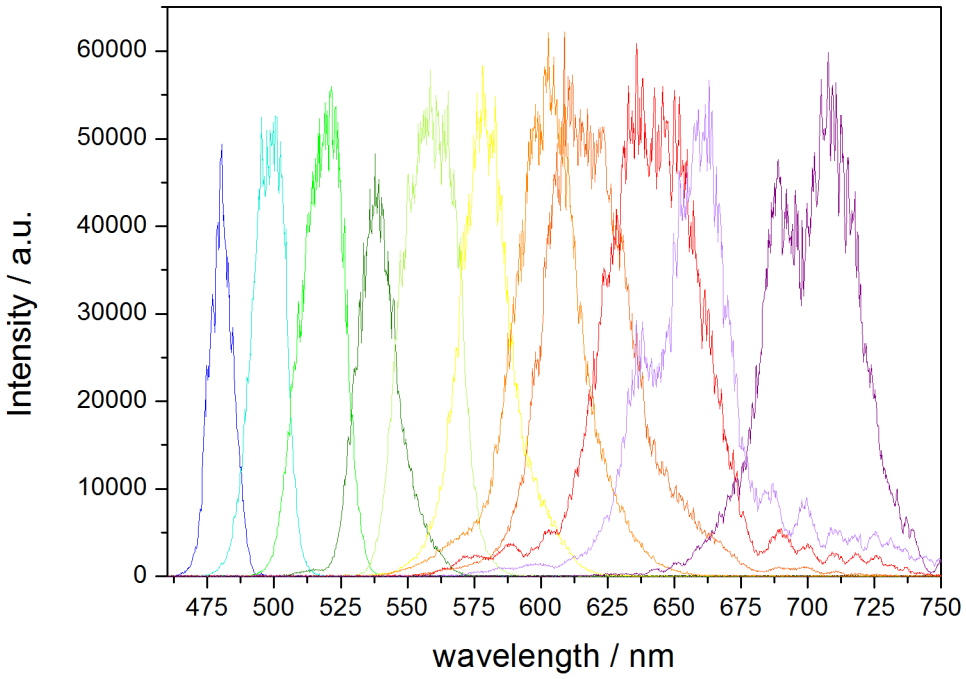


**Figure 3.2:** Examples of amplified pulse spectra generated in a NOPA with central wavelengths from 480 nm to 700 nm in intervals of 20 nm. The bandwidth of the pulses is typically broader where the phase-matching curve is flatter.

The non-colinear geometry of the pulse incidences allows for efficient phase-matching of wavelength components within the white light spectrum with the frequency doubled pump pulse for the entire length of the crystal medium. The relative incident angles of both pulses, the pump light and seed white light, are optimized so that the respective refractive indices for the pump pulse at 387 nm and the wavelength component within the white light spectrum that seeds the parametric amplification process are effectively equal in the propagation direction of the seed in the birefringent BBO medium. Put another way, if

[3]Chirped Pulse Amplifier

the projection of the pump pulse k-vector on the seed pulse k-vector is equal, the pulses remain in phase throughout the crystal medium and maximum parametric amplification is achieved. This configuration allows for fine-tuning of the amplified pulses' bandwidth and has the important advantage that the amplified seed pulse, pump pulse and idler pulse[4] are spatially separated. In a co-linear geometry, the use of dispersive optical elements would have to be used to separate the pulses and cause pulse lengthening. The NOPA has two amplification stages that produce outputs in the order of 20 $\mu$J. Pulses are compressed by a prism pair and pulse durations of sub-40 fs are routinely achieved. A second NOPA is also pumped with a further 30% of the CPA output and allows for pump-probe measurements with both pulses generated in NOPAs. This limits the spectrum that can be measured simultaneously, but improves temporal resolution to sub-50 fs.

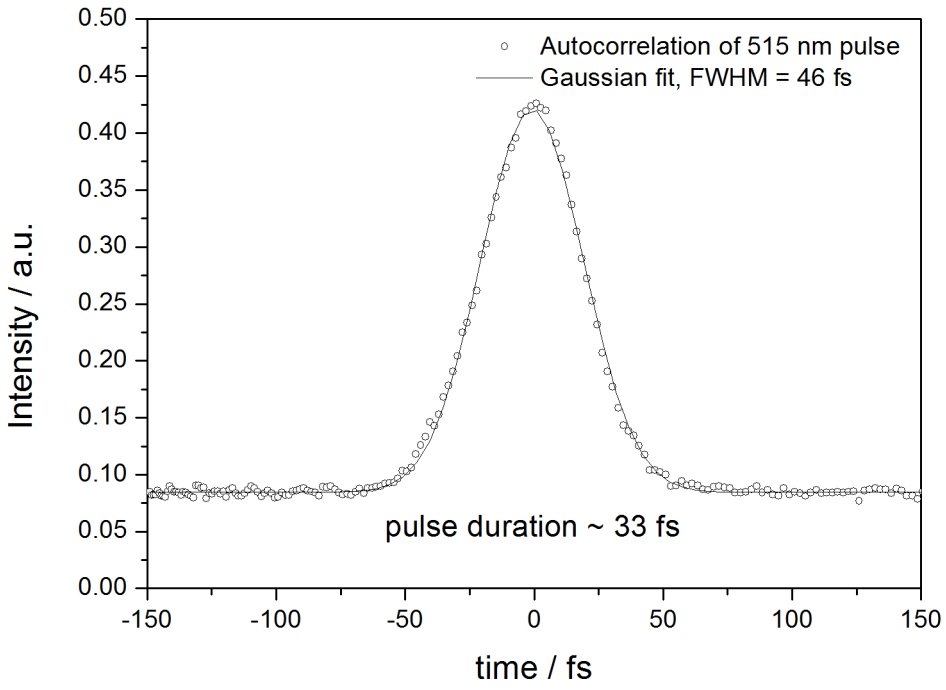


**Figure 3.3:** Autocorrelation of pump pulses centred at 515 nm. Datapoints (open circles) correspond to the second harmonic signal generated by temporal and spatial overlap of reflections of the pump pulse in a non-linear medium (BBO crystal). The measurements were taken with a photo-multiplier tube as a function of delay between the two incident 515 nm pulses. The solid line shows a Gaussian fit to the data corresponding to a full-width at half maximum of 46 fs. Deconvolution of the trace implies a pump pulse duration of 33 ps.

[4]This is the remainder of the photon pair produced when a pump photon is annihilated to produce a duplicate seed photon. The seed photon that overlaps in time and space with the pump in an appropriate non-linear optical medium determines the wavelength and direction of the duplicate, whereas the idler photon has a wavelength determined by energy conservation considerations and a direction determined by momentum conservation.

A further 10%[5] of the CPA output is directed to a white light generation stage, where supercontinua are generated in either a 3 mm sapphire crystal (700 - 440 nm) or a 5 mm $CaF_2$ crystal (700 - 340 nm). Sapphire is preferred as the supercontinuum generated is more stable and greater sensitivity can be achieved. The group velocity dispersion (GVD) experienced by the white light pulse as it propagates from its point of origin in the sapphire or $CaF_2$ crystal to the detector, means the broad bandwidth pulse is positively chirped and is about 1.5 ps in duration when detected. The chirp is observed in the raw data from a measurement such as the one shown in Figure 3.5. The wavelength components that comprise the supercontinuum are spectrally separated in a spectrometer and the temporal resolution is determined by the cross-correlation of the dispersion limited white light pulse and the pump pulse. The temporal resolution can and has been measured in another dissertation [37] by taking the full width at half maximum (FHWM) of the coherent artefact observed during pump-probe overlap in dichloromethane. Here, dynamics like stimulated Raman amplification and cross-phase modulation that give rise to the coherent artefact were observed and the temporal resolution was estimated to be sub-100 fs.

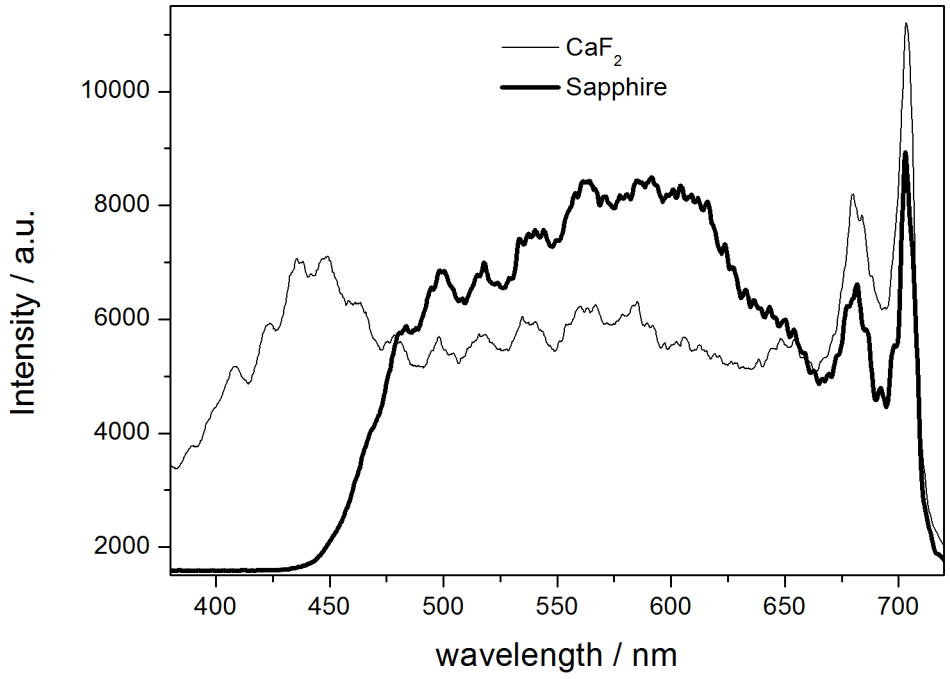


**Figure 3.4:** Probe pulse spectra obtained via supercontinuum generation in Sapphire (thick line) and in $CaF_2$ (thin line).

[5]The remaining CPA output is used for ultrafast electron diffraction experiments.

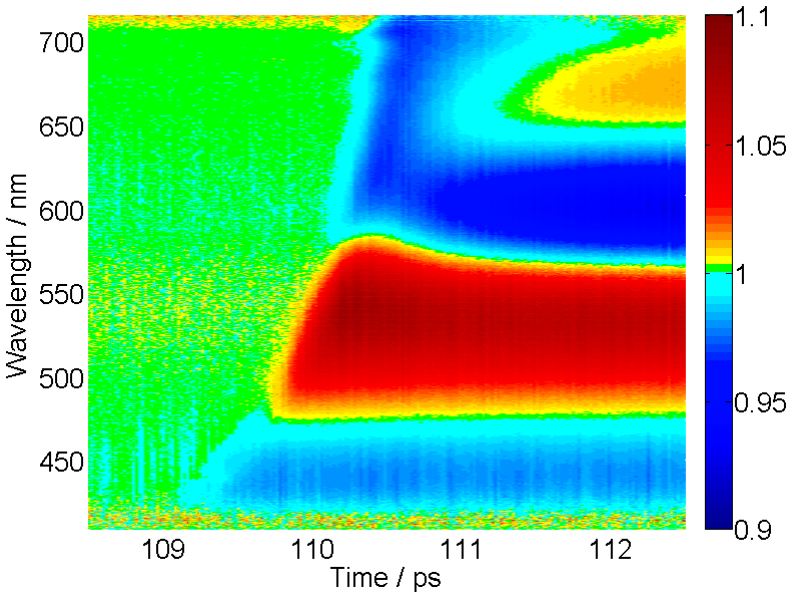


**Figure 3.5:** Example of raw data from a fs-TAS measurement. The chirp of the supercontinuum is seen as the pump pulse is overlapped with different frequency components at different times. The times shown on the axis correspond to delays in the pump beampath. The relative difference in times indicated is correct, but the value shown has no meaning other that we are approximately 110 ps ($\hat{=}$ 33 mm) from the farthest end of the delay stage. The overlap occurs first for shorter wavelengths since the pump pulse beampath is shortened as the measurement progresses to avoid moving parts that can affect detection efficiency in the probe beampath. As such, the pump pulse catches up to the trailing end of the white light pulse first.

The delay between pump and probe pulse is realised by a mechanical translation stage operated by a computer-linked controller (Newport). It can accurately and consistently move $\mu$m, which translates to a few fs. Since the temporal resolution due to the pump-probe cross-correlation is an order of magnitude more, this does not limit the temporal resolution.

## 3.3 Recording data

Data is recorded by an Andor shamrock spectrometer fitted with a 1024 pixel diode array that achieves readout rates of 1 kHz by Entwicklungsbüro Stresing Gmbh. The spectrum of every pulse can thus be recorded individually. When the sample is pumped, the absorption spectrum recorded is a convolution consisting of contributions from molecules in the ground state and those that have been pumped into an excited state. In order to separate the excited state spectrum which is dynamic from the ground state spectrum which isn't, a referencing technique is used. An optical chopper operating at 500 Hz blocks every second pump pulse. Reflected light from a variable neutral density filter, used to regulate the pump pulse energy, is fibre-coupled into a second Andor spectrometer. Both spec-

trometers synchronously read out spectra into a computer. Every alternate white light pulse is the spectrum of the ground state or the convolved transient spectrum which has been excited by the pump pulse. The second spectrometer provides the sorting criteria. In order to elucidate the dynamics of the excited states from the convolved spectrum, the computer is programmed to divide every transient spectrum by the ground state spectrum taken during the next shot when the pump pulse is blocked. Care needs to be taken that the sample decays back into the ground state within the laser period or that a fresh sample is excited with every shot. This technique improves stability and sensitivity since long term fluctuations in pulse intensity is compensated for. The computer programming has a user interface where step size (effectively delay time) for successive measurements and the amount of averaging at each step can be set.

## 3.4 Analyzing data

Now that the data collection has been explained, allow me to elaborate on how it should be interpreted. The measured convoluted spectrum mentioned in the previous section will deviate as a function of time and wavelength from the ground state spectrum, but it may not be obvious since changes in transmission are typically in the order of 1%. After dividing by the ground state spectrum, a transient excited state spectrum emerges. If no change in transmission occurs at a certain wavelength and time, the value will be 1. More transmission will result in a value higher than 1 with the values after the decimal point indicating a percentage change. The opposite is true for an increase in absorption where values will be less than 1. A change in transmission can be due to three different processes:

**Ground State Bleaching** (GSB): when electrons are pumped out of the ground state, less molecules are available to absorb light at wavelengths corresponding to the ground state absorption bands. Here the transmission will increase.

**Fluorescence by Stimulated Emission** (SE): the probe pulse can stimulate the emission of fluorescent photons from excited states back into the ground state. The yield of fluorescent photons at each time step is proportional to the population of the upper state in the radiative transition. Although not as sensitive as time-correlated single photon counting (TCSPC), this is an effective way to determine ps-scale fluorescence lifetimes, provided the intensity is large enough. The fluorescent photons appear as an increase in transmission.[6]

[6]The same is technically true for phosphorescent photons, but the yield and lifetime of these spin-forbidden transitions are typically unsuitable for effective characterization by fs-TAS.

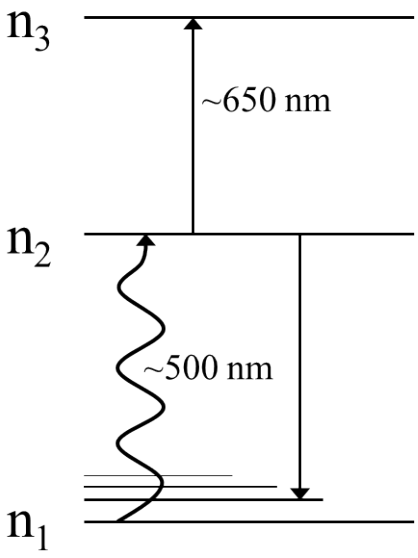


**Figure 3.6:** Energy level diagram of toy model molecule. When in $n_2$ it can either absorb light and populate $n_3$ or decay by fluorescence into $n_1$.

**Excited State Absorption** (ESA): electrons in an excited state may absorb photons at a wavelength corresponding to the energy gap between the excited state and higher-lying states, causing a decrease in transmission at this wavelength.

At this point it may be useful to cement the concepts above with the aid of a toy model. Suppose we have a molecule with 3 discrete states each with their own vibrational manifold. When in the ground state, $n_1$, there are two electronic transitions whereby absorption can take place; $n_2 \leftarrow n_1$ and $n_3 \leftarrow n_1$. Let's say the energy gap between the successive states $n_1$, $n_2$ and $n_3$ is 2.5 eV ($\hat{=}$ 500 nm) and 1.9 eV ($\hat{=}$ 650 nm) respectively - this is of course a totally arbitrary choice. This implies that the absorption bands in the ground state are found at 500 nm and 280 nm, corresponding to transition energies of 2.5 eV and 4.4 eV respectively and that the ground state absorption spectrum would have Gaussian peaks centred at these wavelengths.

Now we excite a certain percentage of molecules in our sample into the $n_2$ state by irradiation with 500 nm light. This is illustrated by the energy level diagram in Figure 3.6. To keep our model simple, we now suppose that the only decay mechanism available to the excited molecules is a radiative transition and that the bottom level is a higher lying vibrational mode of $n_1$. This is only done so that the Stokes shift will separate the absorption and fluorescence[7] signatures spectrally and simplify the analysis of our toy model. Suppose the decay by fluorescence occurs on a 100 ps timescale. Whilst in the $n_2$ state molecules can also absorb 650 nm light and populate $n_3$. Therefore the

[7] Assume the spin quantum numbers of $n_1$ and $n_2$ add up to 0.

excited molecules would have an absorption spectrum with a Gaussian peak at 650 nm and effectively a negative peak at a wavelength slightly red-shifted of 500 nm due to the light emission.

If we measure this toy sample with the setup described in this chapter, we would alternately record the ground state absorption spectrum when the sample is not pumped and the convoluted spectrum of ground state molecules that don't absorb light and the 'certain percentage' of molecules that do, when the sample is pumped - provided the delay between pump and probe is smaller than the decay time of the molecule. The absorption strength of the ground state transitions' contribution to the convolved 'pumped' spectrum will also be less by a measure corresponding to the fraction of excited molecules. For every molecule in an excited state there is one less in the ground state. When these alternate spectra are divided by each other, only the time-dependent excited state spectrum remains along with the ground state bleach - in this case centred around 500 nm and 280 nm.

The data is stored in an $n$ x 1024 matrix with $n$ being the number of datapoints as a function of time (effectively number of timesteps) and the 1024 datapoints comprising the spectrum detected by pixels of the diode array. These datapoints are then converted from their values representing percentage transmission change to a change in optical density ($\Delta OD(\lambda, t)$) in order to adhere to convention. The values are calculated from the following equation,

$$\Delta OD = -log\frac{I}{I_0}, \tag{3.1}$$

where $I$ is the transmission when a pumped spectrum is measured, and $I_0$ is the transmission of the reference ground spectrum. All variables are functions of time and wavelength. In practice an individual pixel in the diode array will record the values for $I$ and $I_0$ as intensity counts for a certain time and wavelength interval, determined by the pump-probe delay and spectrum covering the width of the pixel respectively. The equation is a rearrangement of the Beer-Lambert Law for transmission,

$$T = 10^{-\epsilon \ell c}, \tag{3.2}$$

where $\epsilon$ is the extinction coefficient, $\ell$ is the length of the sample through which light travels and $c$ is the molar concentration. Optical density is the product of $\epsilon, \ell$ and $c$. Rows and columns can be extracted from the $\Delta OD(\lambda, t)$ matrix and decay traces of a spectral signature ($\lambda$ constant) or transient spectrum at a certain time (t constant) can be obtained.

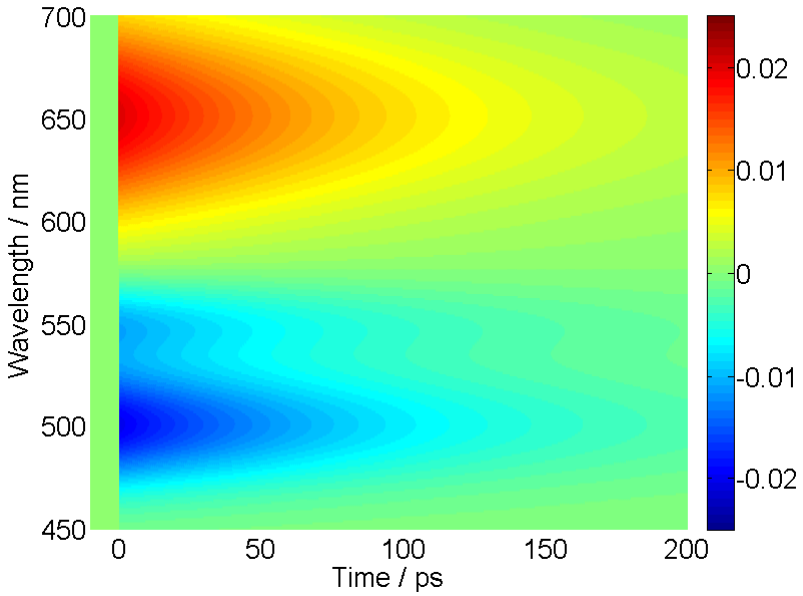


**Figure 3.7:** Simulated transient absorption spectrum of the toy model molecule described in the text. The transient spectrum is plotted as a function of wavelength (y-axis) and time after excitation (x-axis). The data is plotted in a colour scheme quantified by the colourbar in units of $\Delta$OD. The spectral signatures of ground state bleach (GSB) can be seen at 500 nm and fluorescence at 550 nm, both showing an increase in transmission. Whilst the absorption band of the excited molecules shows a decrease in transmission at 650 nm.

Should our toy model be measured and the data stored and processed in this way, the resulting matrix can be seen graphically displayed in Figure 3.7. The colours correspond to changes in optical density, with warm colours corresponding to positive values and cold colours to negative values. The amplitude of the changes in optical density are proportional to the number of excited molecules, the choice of amplitude was random. The ground state bleach signature due to the reduced number of molecules in the ground state can be seen by the decrease in optical density at 500 nm. The same is occuring at 280 nm, but our probe light does not reach this wavelength. We see the fluorescence signal of excited molecules undergoing the $n_2 \rightarrow n_1$ with a Stokes shift of 50 nm at 550 nm. Lastly, the excited state absorption corresponding to the $n_3 \leftarrow n_2$ transition is seen at 650 nm. According to our model that arbitrarily chose the only decay mechanism to have a time constant of 100 ps, all the above signatures decay on this time scale. The amplitudes at any time are then in reality equal in our model; for every photon absorbed, a photon is emitted. Because, in practice, the setup is less sensitive to fluorescence than to absorption, the fluorescence signal amplitude is reduced to reflect this.

When more decay mechanisms are present than in our simple model and spectral signatures overlap, data analysis becomes tricky. Multiple time constants can be extracted from a single signature and these signatures can migrate along the wavelength axis. It

becomes very important in such a scenario to make reasonable assumptions about the kinetics that take place. We will deal with this in the next chapter.

# 4. Results

In Figure 4.1, the stationary ground state absorption spectrum of indoline D149 in a 1:1 solution of acetonitrile and *tert*-butyl alcohol and D149 adsorbed to porous ZnO is plotted. The latter is a solid state sample, deposited on a glass substrate. Effectively, it is the photo-electrode of a D149/ZnO solar cell. The two absorption peaks of the indoline dye solution (dark line) with maxima at 527 and 388 nm correspond to transitions predicted by density functional theory (DFT) calculations [38]. The 527 nm peak is assigned to the $S_1 \leftarrow S_0$ transition and the peak at 388 nm to the $S_2 \leftarrow S_0$ transition. The absorption of ZnO is comparatively weak at wavelengths longer than 380 nm, hence the low efficiency of an unsensitized ZnO solar cell. But as the photon energies start to exceed the bandgap energy of ZnO (3.26 eV), the absorption sharply increases. The peak at 513 nm on the photo-electrode spectrum (grey line), although blue-shifted by 14 nm and broadened, is due to the D149 dye. Likewise, the $S_2 \leftarrow S_0$ transition is broadened and can be seen in the kink in the ZnO bandgap absorption. This broadening has been observed before and is an indication of successful dye adsorption [15]. Although experiments were conducted with

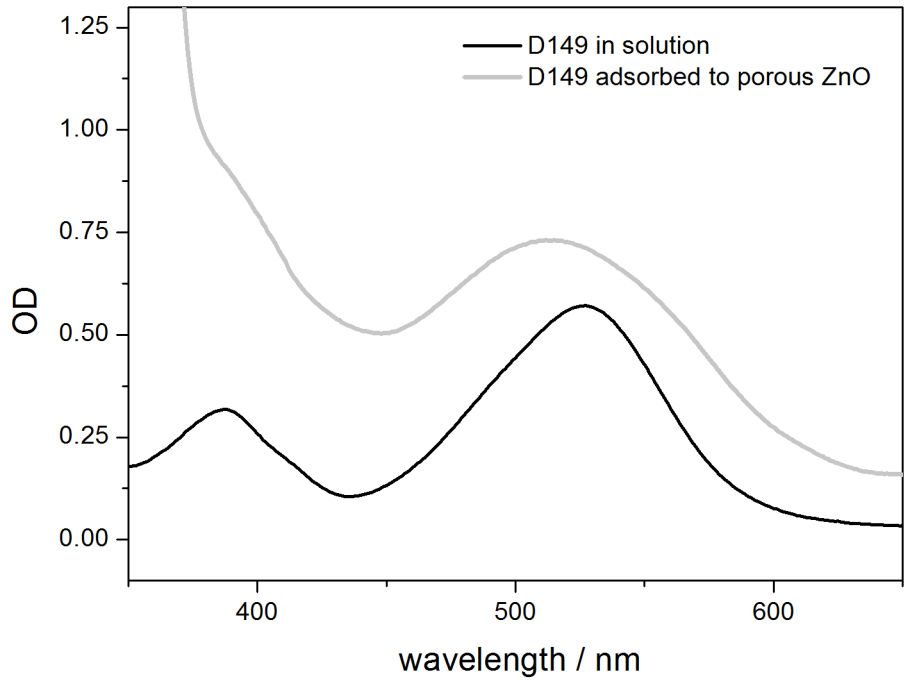


**Figure 4.1:** Stationary absorption spectrum at optical wavelengths of D149 in solution (dark line) and D149 adsorbed to porous ZnO (grey line).

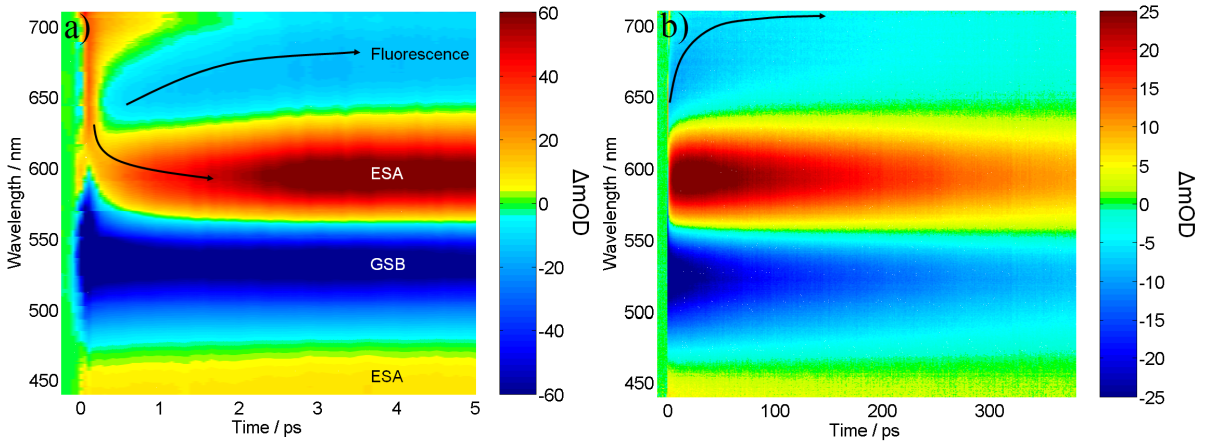


**Figure 4.2:** Transient spectra of D149 in a 1:1 volume solution of acetonitrile and *tert*-butyl alcohol. Data was recorded in 50 fs intervals over a range of 5 ps in (a), whilst intervals of 1 ps over a range of 350 ps resulted in (b). The transient signatures attributed to fluorescence by stimulated emission, ground state bleaching (GSB) and excited state absorption (ESA) are labelled in (a). The arrows in both spectra indicate the trajectory of the migrating band maxima as a function of time and wavelength.

excitation at both absorption peaks of D149, no appreciable differences were observed in the transient data. The results presented in this chapter will be from data sets where excitation occurred at the $S_1 \leftarrow S_0$ transition. The first singlet excited state lies above the conduction band edge and since ZnO has negligible absorption at this wavelength, we are sure to deposit the pulse energy in the dye molecule.

## 4.1 fs-TAS of D149 in solution

In order to understand the photodynamics of the dye in a functioning DSC, we will first need to understand the photodynamics of the dye itself. D149 in a solution of 1:1 acetonitrile and tert-butyl alcohol was pumped through a sapphire flow cell of 200 $\mu$m thickness at a sufficient rate that each laser shot excited a fresh volume of dye solution. The NOPA was tuned to 530 nm and produced 70 $\pm$ 10 nJ pulses of 30 $\pm$ 5 fs duration. These pulses are focused on a spot size of 150 - 200 $\mu$m diameter. Taking all of this into account implies the samples are subject to incident intensities of 3 - 4 GW/cm$^2$. According to our experience and observations, this seems to be well within the linear excitation regime, since in the order of 1% of molecules within the pump volume are excited by the pump pulse. Both pulses are linearly polarized set at a relative angle of 54.7°, the 'magic angle', in order to desensitize the measurement to rotational decoherence [39]. The probe pulse after supercontinuum generation in sapphire or $CaF_2$, is collimated by a parabolic mirror and subsequently focussed with an achromatic lens to a spot size diameter below

50 $\mu$m in the sample. The probe pulse is much smaller in diameter at overlap than the pump. This results in improved stability since small errors in beam alignment, that could cause imperfect spatial overlap of equally sized beams as the translation stage is moved, are compensated for.

Figure 4.2 shows two transient absorption spectra describing the photodynamics of D149 in solution on different timescales. The higher temporal resolution spectrum on the left was recorded in 50 fs intervals over 5 ps. The spectrum on the right measured the ps - scale dynamics. These 2 dimensional plots use a colour scheme to represent optical density changes as a function of wavelength on the vertical axis and pump-probe delay time on the horizontal axis. Warmer colours indicate increased absorption ($\Delta$OD $> 0$), colder colours indicate an increased transmission ($\Delta$OD $< 0$) whilst green indicates no change relative to the ground state spectrum ($\Delta$OD $= 0$).

The pump light at 530 nm causes a partial depletion of the ground state which results in less absorption at all ground state absorption bands. The absorption band observable within the probe light spectrum is the $S_1 \leftarrow S_0$ transition centred around 530 nm, and indeed here we see ground state bleaching (GSB). Signatures of increased absorption are centred about 600 and 450 nm from 1 ps after excitation; features of ESA to separate higher-lying electronically excited states ($S_m$ and $S_n$ in Figure 4.3). The increase in transmission observed in the spectral region between 650 and 700 nm does not correspond to a ground state absorption band and is due to stimulated emission of fluorescent photons by the probe pulse. The fluorescence is visible to the naked eye in solution[1].

These features show spectral dynamics on different timescales. On the sub-ps scale we see a broadband ESA that stretches from the edge of the GSB signal to the red edge of the observable spectrum. Within the first picosecond the ESA maximum shifts from 620 nm to 600 nm. Also within the first picosecond, but after a few hundred femtoseconds, the fluorescence signature emerges from its early superposition with the broadband ESA. On the scale of a few ps, the fluorescence band maximum red-shifts from 640 to 660 nm within 4 ps and the ESA continues to shift albeit at a slower rate and reaches a stable maximum at 600 nm. The measurement taken with ps steps, reveals a continued red-shift of the fluorescence band maximum until it reaches 700 nm after 100 ps. Horizontal lineouts at the ESA and fluorescence maximum show a maximum $\Delta$OD after 18 ps - this is an artificial rise in signal resulting from better spectral separation of the two migrating bands.

The broadband ESA is interpreted as the absorption of the vibrationally hot $S_1$ states,

[1] Although counter-intuitive, a good light emitter is often a sign of a good light absorption material for solar cells. A high fluorescence yield implies an absence of competing fast non-radiative pathways and dark states that lead to a reduced photovoltage.

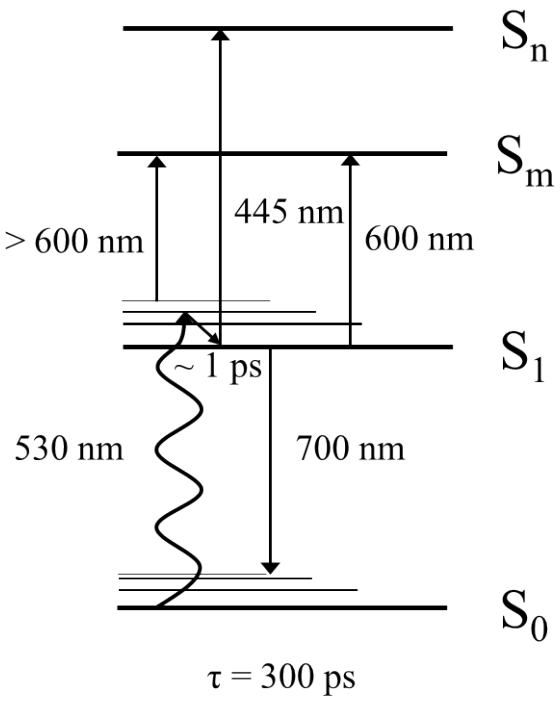


**Figure 4.3:** Simple energy level diagram mapping the transitions of D149 in solution. Ground state bleaching is observed at the 530 nm transition. The $S_1$ state absorbs at 445 nm and 600 nm. In the latter case excited state absorption is initially broadband due to absorption by hot vibrational states but these cool on the scale of 1 ps. Fluorescence is seen at 700 nm. The signatures of GSB, ESA and fluorescence decay with a 300 ps time constant.

their quick decay within 300 fs at wavelengths longer than 620 nm and ultrafast blue shift is interpreted as vibrational cooling of the excited wavepacket. As higher vibrational modes of the $S_1$ state depopulate and the ground vibrational state is populated, the wavelength shortens since the transition to higher lying states becomes energetically greater. The subsequent simultaneous blue-shift of the ESA and red-shift of the fluorescence maximum both indicate a lowering of the energy of the excited state and may be partially due to vibrational cooling still. However, the timescale of this dynamic, typical of rotation and reorientation of molecules, suggests solvation dynamics may be responsible. This term refers to the reorganization of the dielectric environment[2] that the excited molecule finds itself in as a response to the change in dipole moment resulting from excitation. The known large change in dipole moment in the case of the $S_1 \leftarrow S_0$ transition in D149 [38] suggests that this effect should be pronounced. The ESA band absorbs strongly around 600 nm after a few ps. This is the absorption of the ground vibrational mode of the $S_1$ excited state.

The shifting spectral position of the fluorescence maximum with time was fitted with

[2] consisting in this case of individual solvent molecules

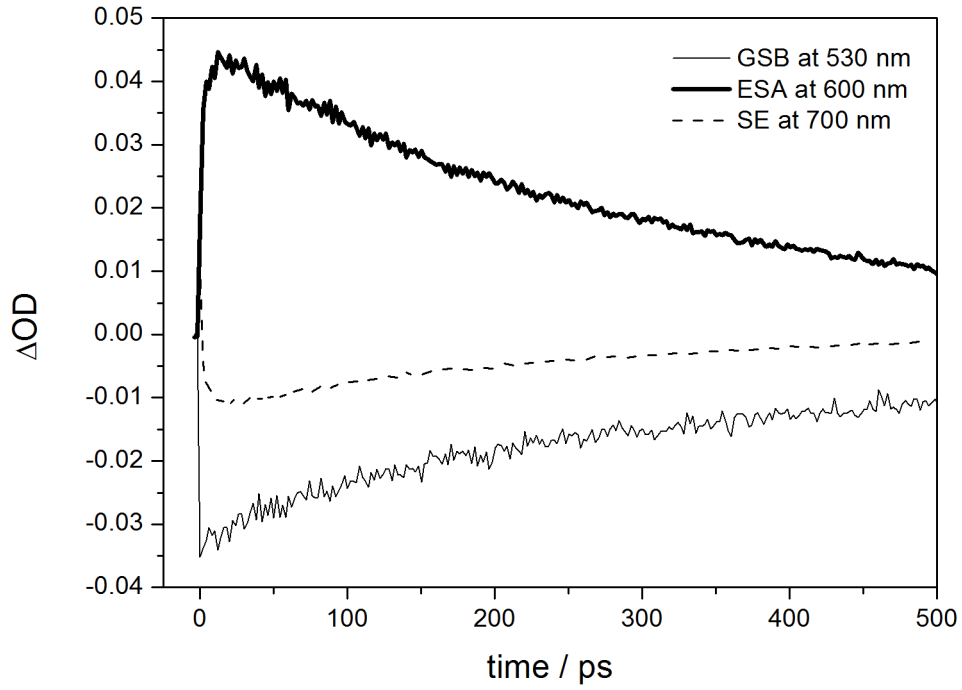


**Figure 4.4:** Decay traces taken at the Excited State Absorption maximum at 600 nm (thick line), Ground State Bleach maximum at 530 nm (thin line) and the steady state fluorescence maximum at 700 nm detected by Stimulated Emission (dashed line). All traces were averaged over a 15 nm spectral window. The slow rise time of the ESA and SE signals compared to GSB are due to their spectral overlap at early times.

exponential function and produced a time constant of 40 ± 10 ps. The lifetimes of the photo-initiated processes were extracted from decay traces at 530 nm (GSB), 600 nm (ESA) and 680 nm (Fluorescence). These traces, shown in Figure 4.4, were fitted with mono-exponential decay functions and revealed common decay times of 300 ± 50 ps. The ground state thus recovers at the same rate as the $S_1$ population decays and the fluorescence signal diminishes. This observation indicates that the $S_1$ state decays directly into the ground state and that it does so predominantly by fluorescence. These dynamics are summarized by the illustration in Figure 4.3. In a paper published shortly after these measurements were taken, Lohse et al [40] investigated the photodynamics of D149 in different solvents. They observed a fluorescence shift and fitted it with an 19 ps time constant in methanol and acetonitrile. They reported solvent polarity-dependent $S_1$ decay times. Amongst others, the solvents acetonitrile and methanol were used and yielded decay times of 280 ± 10 ps and 99 ± 5 ps respectively, in good agreement with our results considering *tert*-butyl alcohol is less polar than acetonitrile and methanol.

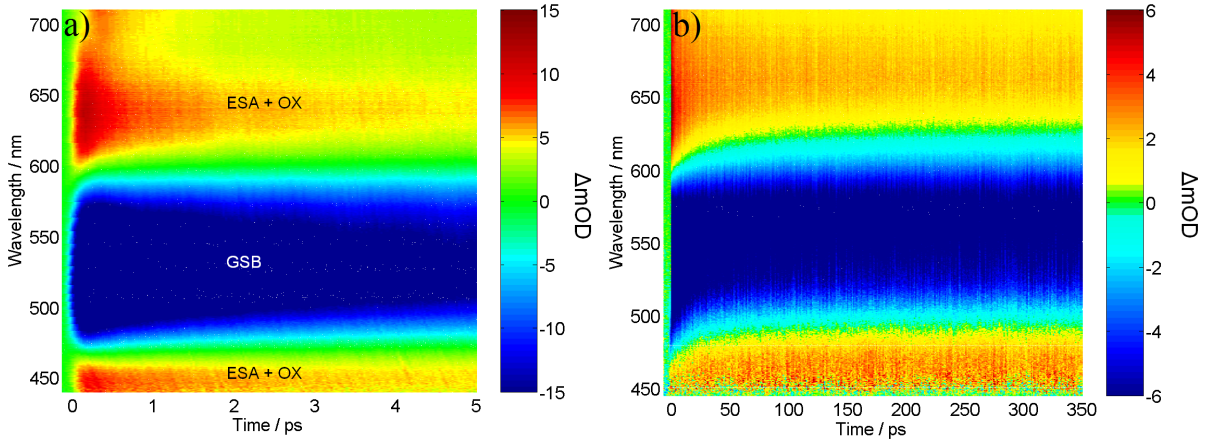


**Figure 4.5:** Transient spectra of D149 adsorbed to the porous ZnO photo-electrode. Data was recorded in 50 fs intervals over a range of 5 ps in a) whilst intervals of 1 ps over a range of 350 ps resulted in b). Compared to the dynamics of the dissolved dye, the absence of a fluorescence signal is apparent. The excited state lifetime is also drastically reduced and decays significantly faster than the ground state recovers, indicated here by the label GSB.

## 4.2 fs-TAS of D149 adsorbed to a porous ZnO network

Before we get to the dynamics of the complete DSC, we will investigate the photo-electrode alone as an intermediate step. As mentioned before, the photo-electrode consists of a near-monolayer of D149 adsorbed to the surface of a highly porous ZnO network. The experiments were conducted under identical conditions except that the pump and probe polarization were set parallel since the sample is now in the solid state and the molecules do not rotate freely. The samples were also translated along a circular path during the measurement to avoid photobleaching of the sample during prolonged measurements.

In Figure 4.5 the transient spectra of the D149/ZnO photo-electrode are presented. The absence of the fluorescence band signature and the severe quenching of the ESA are perhaps the most evident changes. Although encouraging, the absence of detectable fluorescence is insufficient to suggest conclusively that charge transfer is taking place. The fact that the D149 molecule now finds itself in the solid state is enough to explain this effect. The solid state opens up a plethora of radiationless relaxation pathways.

The decay trace of the ESA maximum at 650 nm, binned and averaged over a 15 nm band, is presented in Figure 4.6 and was fitted with multi-exponential functions on both timescales. It is compared with the ESA signature decay trace of D149 in solution at 600 nm to highlight the contrast. The difference in ESA maximum wavelength may be due to the fact that the dye molecules are now sterically constrained as opposed to the situation where the ESA band shifts to lower energies (as indicated by the blue-shift of the ESA band) when the dye is in solution. The solvent molecules, in such a case, respond to the

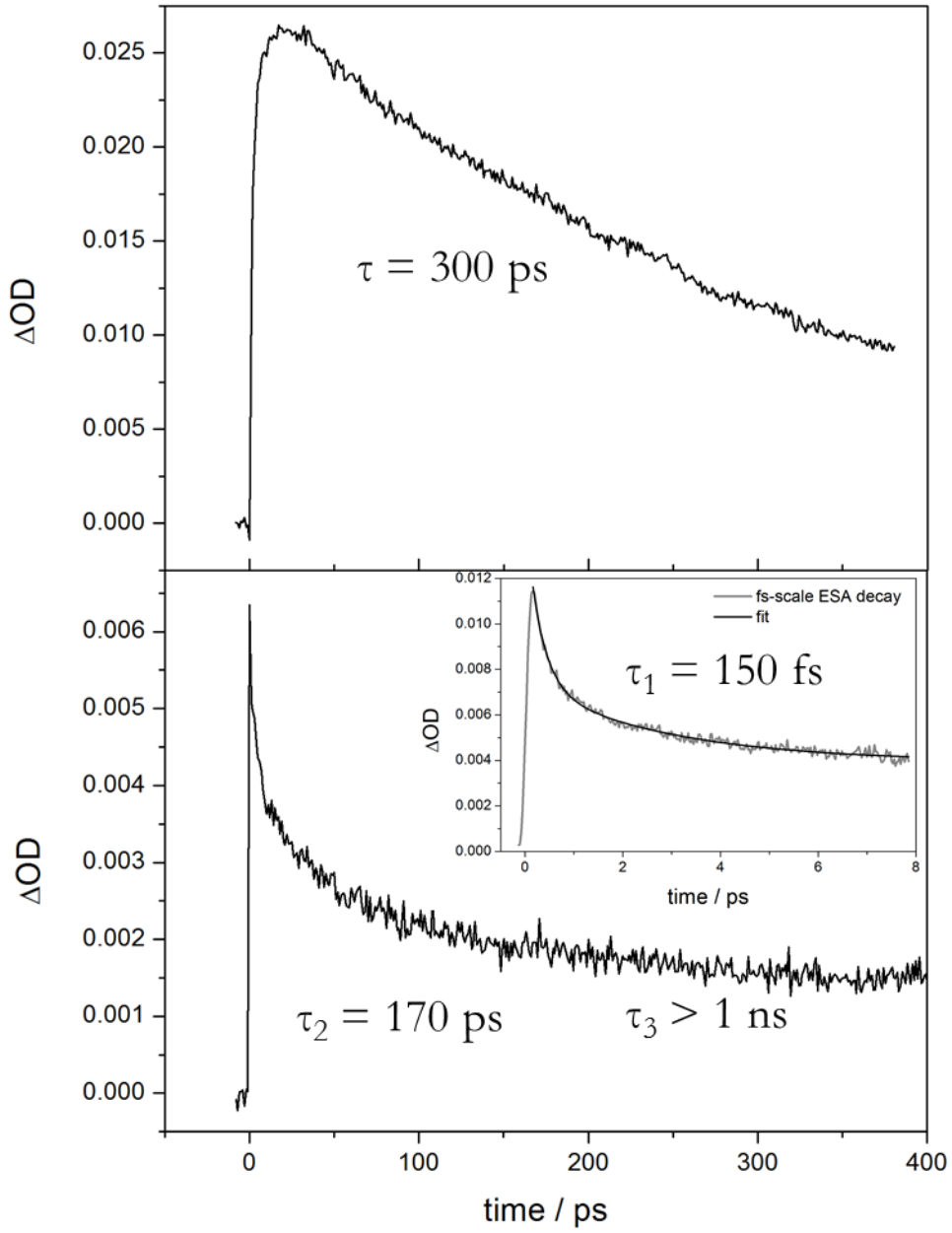


**Figure 4.6:** Direct comparison of the ESA band maximum decay signatures on a ps-timescale of D149 in solution at 600 nm in (a) and of D149 adsorbed to a ZnO photo-electrode at 650 nm in (b). The inset in (b) shows the ultrafast component of the ESA decay when adsorbed to ZnO from a separate highly time-resolved scan. The decay in (a) is fitted with a mono-exponential decay function with a time constant of 300 ± 50 ps. The decay in the adsorbed photo-electrode case is fitted with a multi-exponential decay function with an ultrafast component of 150 ± 20 fs, a ps-scale component of 170 ± 20 ps and a long-lived component in the ns-regime that cannot be reliably fitted with the available data.

excitation and accompanying change in dielectric moment to lower the potential energy of the excited state.

The decay trace in the case of the photo-electrode on the ps scale was averaged over multiple measurements and consistently revealed time constants of 170 ps and a long-lived component larger than 1 ns. A dominant ultrafast component was observed throughout the 580 to 700 nm region and fitted with a decay constant of 150 fs ($\tau_1$) at the 650 nm band maximum. The ESA feature at 450 nm could be fitted with the same decay constant as the ESA band at 650 nm, but the decay is weighted towards the longer components. The GSB signal hardly recovers on the scale of a few ps, but shows decays with time constants 170 $\pm$ 20 ps ($\tau_2$) and a longer ns-scale component ($\tau_3$).

These observations, along with the fact that the cell has a known high quantum yield of injected electrons from IPCE measurements [29][3] and the fact that the DSC works at all, make a great case that we are observing charge transfer dynamics. The ultrafast 150 fs ($\tau_1$) decay seen in the ESA is faster even than the vibrational cooling observed with the dye in solution, a possible reason for the improved spectral separation of the ESA and GSB features in the photo-electrode transient spectrum. This component is not mirrored in the GSB decay trace, implying that although the population of the excited state rapidly decreases, the ground state does not repopulate. For this reason this component is attributed to electron injection from the dye's excited state to the conduction band of ZnO. The decay is three orders of magnitude faster than the relaxation seen in solution. It has to be in order to compete with other decay mechanisms and still produce the measured large charge injection quantum yield. The 170 ps component ($\tau_2$) is also found in the ground state recovery and is thus attributed to the geminate recombination of dye molecules not undergoing charge transfer, facilitated by radiationless decay mechanisms like phonon-coupling.

From Literature we know that the oxidized D149 molecule has red-shifted absorption bands at 450 and 650 nm [41,42], which overlap exactly with the ESA bands of the neutral dye molecule. Hence the labelling in Figure 4.5 of the superposition as ESA + OX. See traces at these wavelengths in Figure 4.7. The oxidized D149 absorption band explains the long lived ns-scale component observed in the bands labelled ESA + OX and GSB. The GSB signal remains until the ground state of the neutral molecule recovers. Since the sample measured here consists solely of the photo-electrode, the long $\tau_3$ components are a measure of the non-geminate recombination rate of injected electrons in the semiconductor back to the ground state of the dye. The diffusion of electrons back to the D149/ZnO interface is the only source of electrons for regeneration of the neutral dye in a closed

[3] see also Figure 2.3

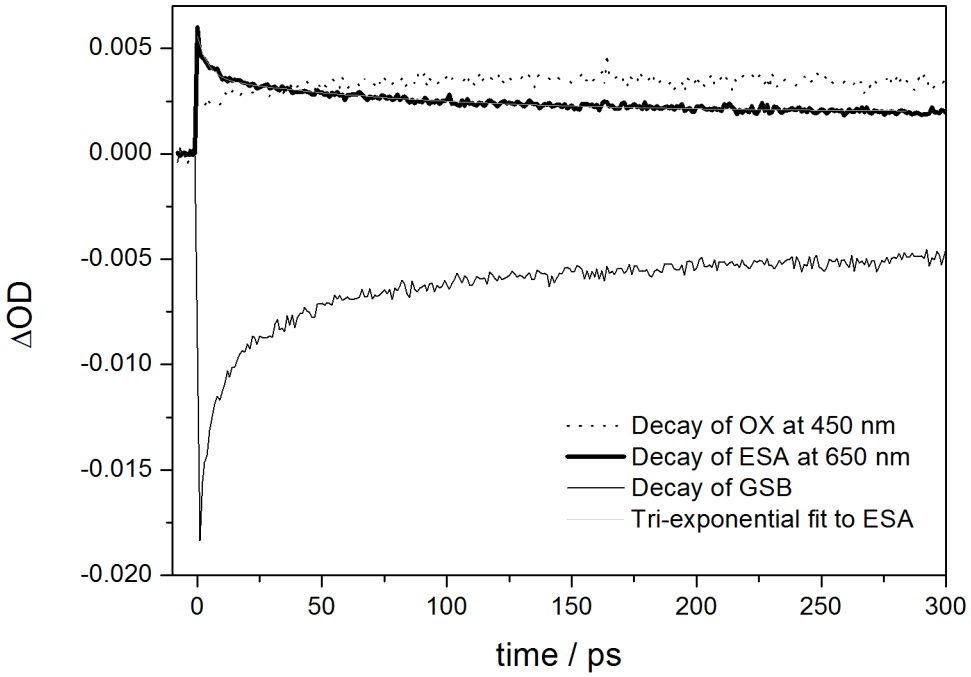


**Figure 4.7:** ps-scale Decay traces of ESA, GSB and OX at 650, 530 and 450 nm respectively. Each averaged over 15 nm. The 150 ps scale decay of the ESA is mirrored by the GSB indicating a geminate recombination process. The relative intensities of these signals have changed; the GSB dominates in absorption strength, due to the fs scale charge injection out of the excited state. The signature at 450 nm is weighted heavily towards the emerging long-lived absorption of the oxidised molecule.

system as is presently the case. This long decay component indicates a longer-lived charge separated state, consistent with the proposed charge transfer mechanism.

## 4.3 fs-TAS of complete D149/ZnO DSC

The next step will be to add an electrolyte to the system, completing the DSC. An identical experimental setup was used as before and the measurements presented in this section were done under open circuit conditions. The subtle differences are not easily discernible from the 2D transient spectra. Differences in the lifetimes of the main transient features were seen in the ESA+OX bands presented in Figure 4.8. To extract a decay constant, the band at 450 nm was fitted. The band is a convolution, as mentioned in the previous section, of the ESA of the $S_1$ state and the absorption of the oxidized dye molecule and is weighted more to the oxidized signal at 450 nm.[4] Analysis of these traces revealed a shorter $\tau_3$ component in the order of 1 ns. We conclude that the faster regeneration of

[4]For the same reason, the 650 nm band was used to extract excited state lifetimes.

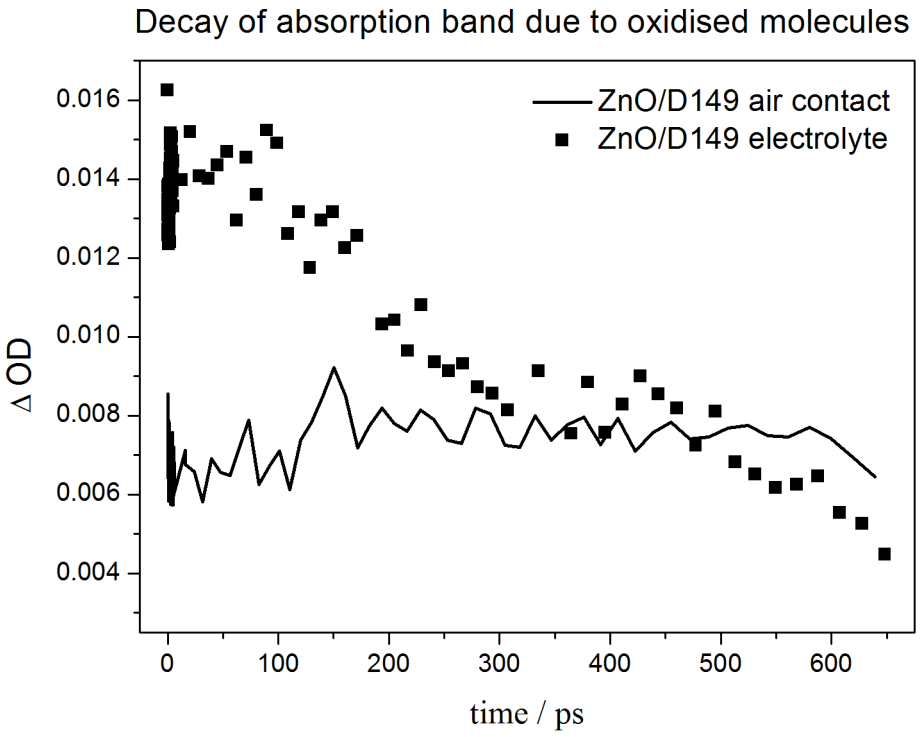


**Figure 4.8:** Decay trace of the absorption signal of the dye in it's oxidized state at 445 nm for the D149/ZnO photo-electrode exposed to air (solid line) and exposed to an electrolyte (dark squares). The redox couple accelerates the decay to in the order of 1 ns. This indicates accelerated recovery of the neutral state of the dye by the action of the electrolyte that intercepts the recombination of electrons in the conduction band with the holes in the HOMO of the dye.

the neutral dye is due to the action of the redox mediator dissolved in the electrolyte that intercepts the non-geminate recombination.

This completes the characterization of the photodynamics of D149 at visible wavelengths in different environments; in solution, adsorbed to ZnO and in a complete D149/ZnO cell. In the latter case, the dynamics of excited state absorption, ground state bleaching and absorption by oxidized molecules created by charge transfer, have been identified and their action characterized on different timescales. The remaining sections and subsections in this chapter will deal with how these specific signatures and the processes they describe are affected by material selection, production protocol and external parameters that may affect the cell during operation.

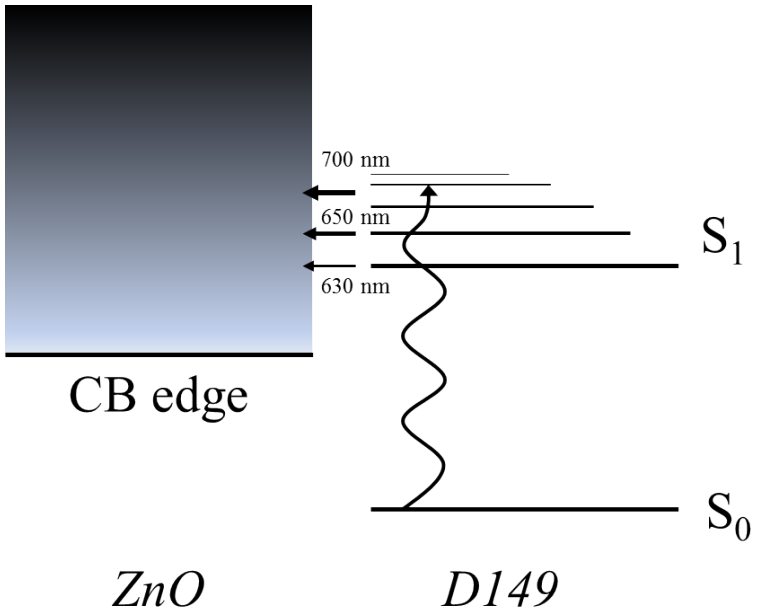


**Figure 4.9:** Energy level diagram representing charge injection in a D149/ZnO DSC. Vibrationally hot $S_1$ states couple with a higher density of states in the conduction band (CB) of ZnO. Thicker arrows indicate higher injection rates. Longer wavelengths correspond to the absorption of higher energy states. The wavelengths compared in this subsection are indicated.

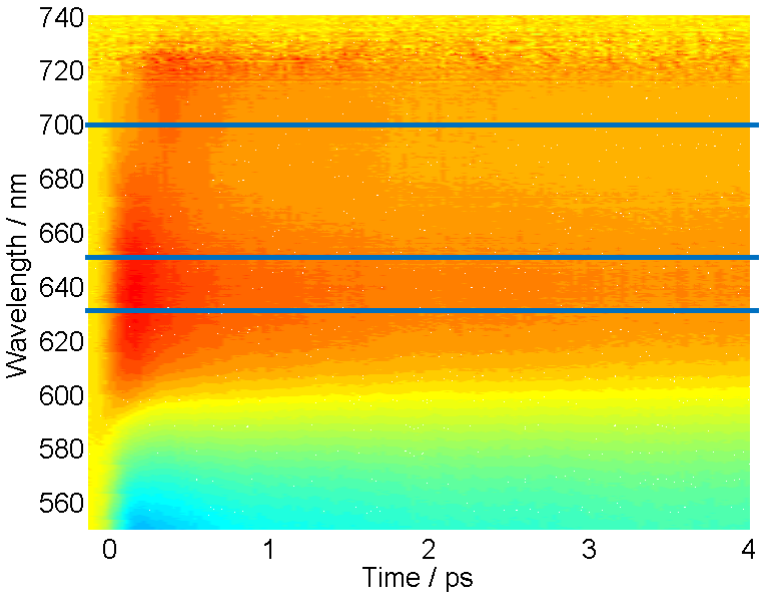


**Figure 4.10:** fs-TAS of D149/ZnO cell, with the ESA band enhanced. Ground $S_1$ vibrational state absorbs at 630 nm; this is compared with the absorption of vibrationally hotter states at 650 nm and 700 nm. The traces extracted for comparison are indicated by thick blue lines.

## 4.4 Further effects

### Incident wavelength dependence of electron injection

The shape of the D149/ZnO IPCE[5] spectrum resembles the absorption profile of D149 at visible wavelengths. Compare Figure 2.3 with Figure 4.1. From this it is evident that the LHE[6] is a major contributing factor to the overall efficiency. The question arises whether the excitation wavelength also results in different charge injection efficiencies? It may be useful at this point to consult Equation 1.3. Higher excitation energy may result in hotter vibrational $S_1$ states that couple with a higher density of states above the conduction band edge of the semiconductor and may, as a result, inject electrons at a higher rate. This is visually conceptualized in Figure 4.9. A fs-TAS spectrum is plotted in Figure 4.10 to show what the broadband ESA looks like and where the traces presented in this subsection were taken from. These traces are also represented for clarity in Figure 4.9. Indeed this effect is observed in all samples. Figure 4.11 shows the electron injection signature at the band maximum and for two wavelengths red-shifted of the band maximum, which correspond to the absorption of vibrationally hot $S_1$ states[7]. Here the trend is evident; injection proceeds faster in hotter vibrational states and competes with vibrational cooling. This is in line with previous observations on a perylene/$TiO_2$ DSC [43].

This can also be seen in the slight changes in the ESA spectrum when different electronic transitions are pumped. The ESA spectrum is plotted in Figure 4.12 for a D149/ZnO photo-electrode excited at 388 nm corresponding to the $S_2 \leftarrow S_0$ transition and at 530 nm, the absorption maximum of the $S_1 \leftarrow S_0$ transition. The ESA spectrum at the point where the signal is greatest for the 388 nm pumped sample is 380 fs after excitation. Presumably this is because the $S_2 \rightarrow S_1$ deactivation needs to occur first, it is reported to be sub-picosecond [40]. The ESA spectrum, when pumped with 530 nm, shows greater absorption closer to overlap (t=0). The ESA spectrum in the latter case is weighted more towards the band maximum, while the sample pumped with higher photon energy (388 nm) shows a smoother spectral profile, weighted more evenly with longer wavelengths.

It is therefore perhaps prudent to include a caveat at this point by mentioning that in the comparisons made in other sections of this chapter, the band maximum is always considered. The spectral position of this maximum, believed to be the ground vibrational mode of the $S_1$ state since it outlives the others, may change from sample to sample depending on its environment. However, when the same sample is excited with different wavelengths, thereby populating vibrationally hot states differently, the injection time at

[5] Incident Photon to Current conversion Efficiency
[6] Light Harvesting Efficiency
[7] lower transition energy to upper level

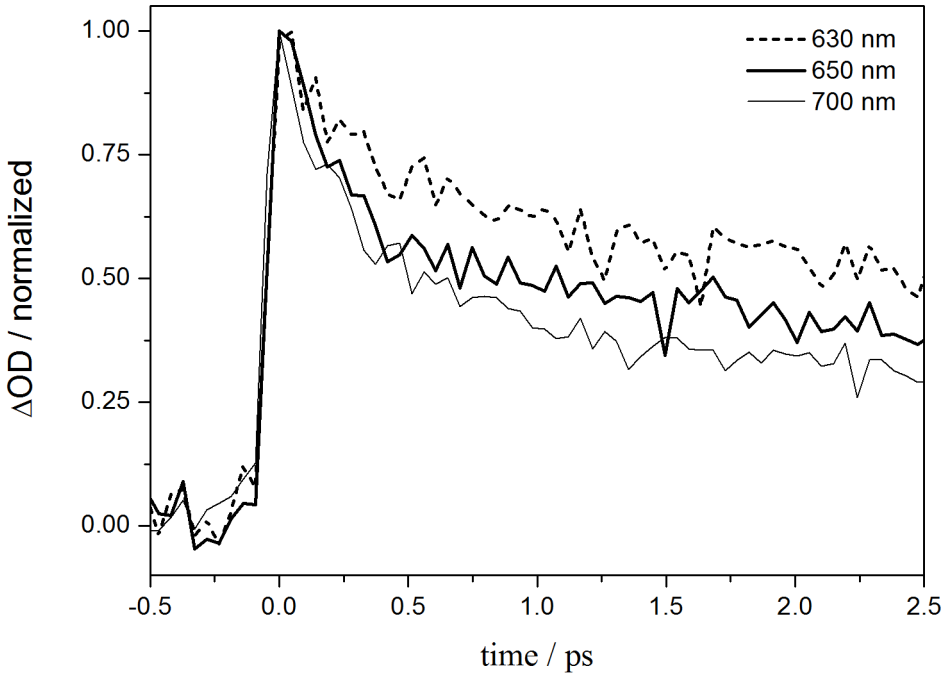


**Figure 4.11:** The ESA decay traces at different wavelengths extracted from the same transient spectrum suggest vibrationally hot states inject at a greater rate. The band maximum corresponding to the vibrational ground state is found at 630 nm (dotted line). The vibrationally hotter states absorb at longer wavelengths, represented here by traces at 650 nm (thick line) and 700 nm (thin line). The decay traces are normalized to emphasize the change in injection time, but have relative ΔOD values shown in the transient spectrum in Figure 4.12.

the band maximum remains unchanged, since in all cases it is proportional to the ground vibrational $S_1$ state's coupling with the conduction band of ZnO. This is seen in Figure 4.13 where the injection rate at 650 nm is unaffected by the change in incident wavelength on the same D149/ZnO photo-electrode. A D149 sensitized ZnO photo-electrode was excited in 2 separate experiments at the 530 nm absorption maximum and in the blue flank of the absorption band at 500 nm. The electron injection signature at 650 nm is compared. The data suggests that the injection rate for the ground vibrational $S_1$ mode is independent of incident photon energy.

There is thus an incident wavelength dependence of electron injection efficiency[8] within the absorption band. This, however, needs to be weighted with the LHE which is wavelength dependent when considering IPCE values. Hot vibrational states may inject slightly faster, but cooler vibrational states are better populated due to higher absorption cross-sections.

[8] can also be interpreted as the degree of orbital coupling

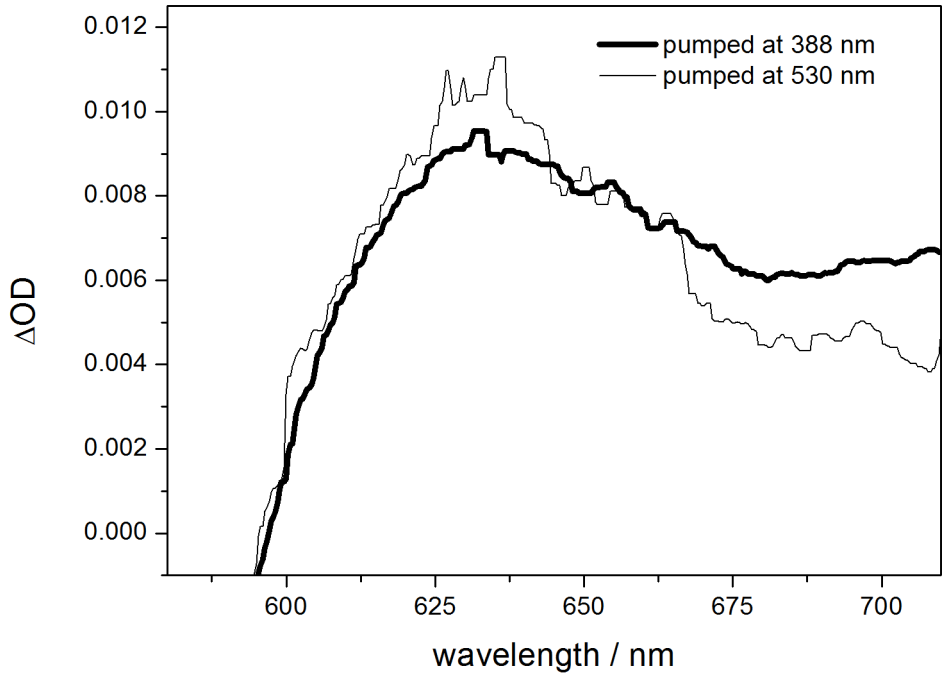


**Figure 4.12:** Transient ESA spectrum at maximum ΔOD of D149/ZnO photo-electrode after $S_2 \leftarrow S_0$ excitation (thick line) and after $S_1 \leftarrow S_0$ excitation (thin line). The higher energy transition shows a smoother population distribution with more electrons in higher lying vibrational modes.

## Photodynamics of charge transfer in open atmospheric vs inert conditions

The importance of measuring photo-electrodes under inert conditions was demonstrated in a control experiment where identical photo-electrodes were measured with one exposed to air and the other encapsulated with a glass plate and filled with $N_2$ gas. When comparing the transient spectra at different times, the red-shift of the spectral signatures with time becomes apparent for the sample exposed to air (see Figure 4.14). In the case of the sample under inert conditions, this effect is severely limited. When comparing the GSB signal, we note that the ground state recovers slightly faster for the sample exposed to air. A difference in injection times ($\sim$ 100 fs) is not seen, but may be too marginal to detect. Oxygen and water molecules in the air are the most likely candidates to react with the ZnO surface and donate electrons to oxidized D149 molecules accounting for the faster regeneration rate.

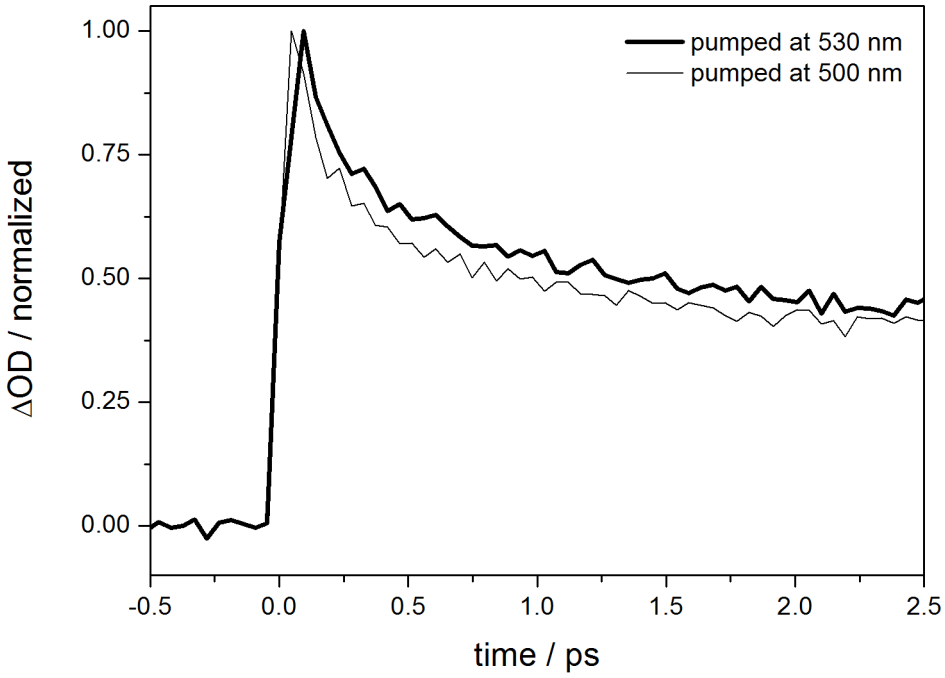


**Figure 4.13:** ESA decays at 650 nm of the same D149/ZnO photo-electrode excited at the absorption maximum (530 nm, thick line) and at the blue flank of the absorption band (500 nm, thin line). The decay signature is assigned to the coupling between the ground vibrational mode of the D149 $S_1$ state and the conduction band of ZnO resulting in charge transfer and the dynamics here do not show an incident wavelength dependence.

## Electron injection under operating conditions

Several experiments were conducted to determine the effect of an external circuit attached to the cell on the observed photodynamics. The photo-electrochemical characterization (see Figure 2.2) revealed that the current stops flowing when a bias potential of between 0.6 and 0.7 V is applied. Additionally, a practically constant maximum current density under short circuit conditions and in the applied bias potential range up to 0.4 V is observed.

The purpose of the inquisition discussed presently, is primarily to establish whether the observed change in macroscopic cell parameters translates on a molecular scale to a reduction in dye-to-semiconductor electron injection efficiency.

Despite several attempts with applied voltages in both directions and in some cases far beyond $V_{OC}$, the primary electron injection efficiency was unaffected. This is seen in Figure 4.15. In response to concerns that the temporal resolution of the NOPA-pumped/Supercontinuum-probed setup was insufficient to resolve subtle changes in charge

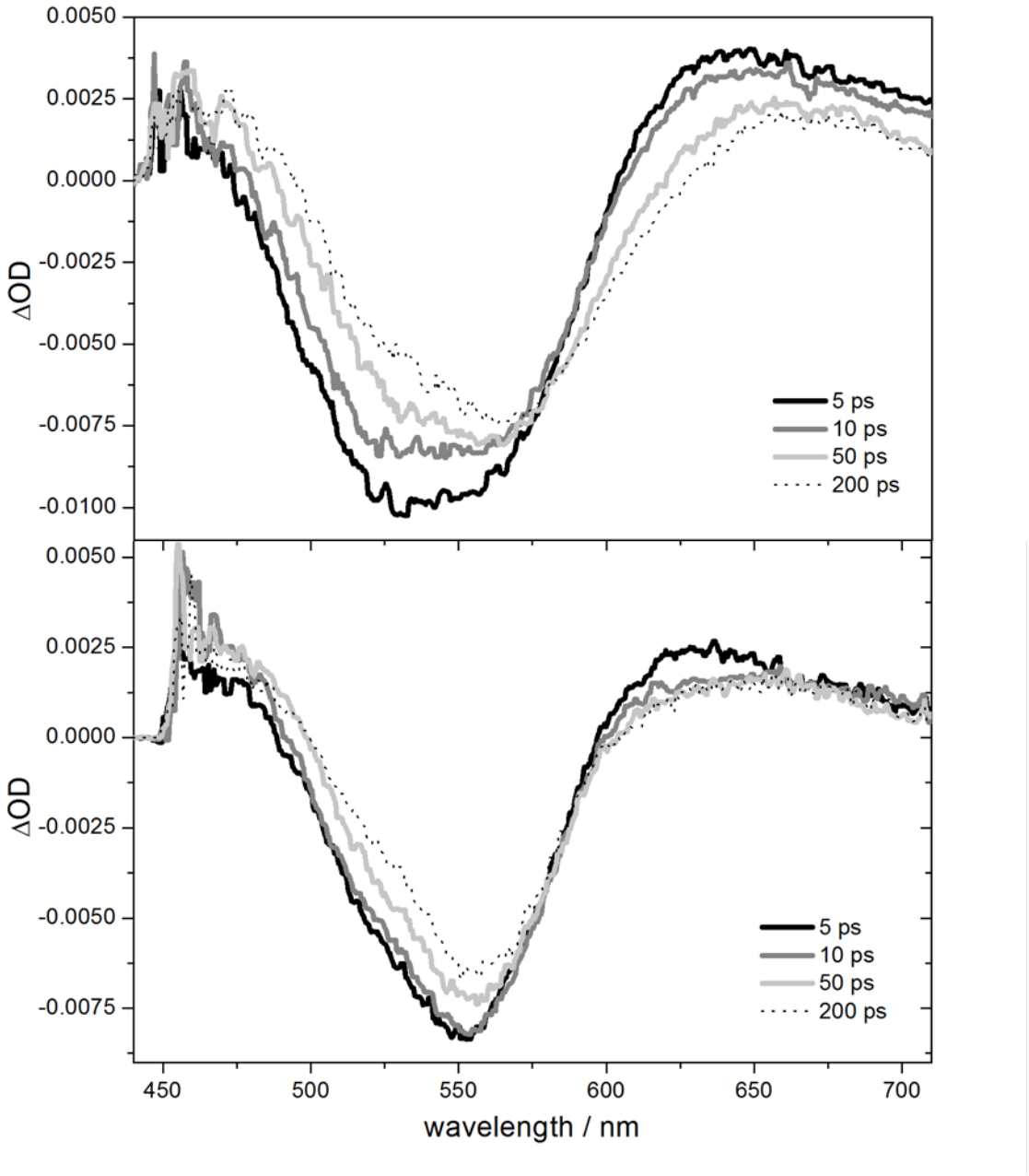


**Figure 4.14:** Transient spectra are plotted at intervals 5, 10, 50 and 200 ps after excitation for D149/ZnO photo-electrodes exposed to ambient atmosphere (top) and to inert $N_2$ (bottom). In the sample exposed to air the isosbestic points shift to longer wavelengths with later times.

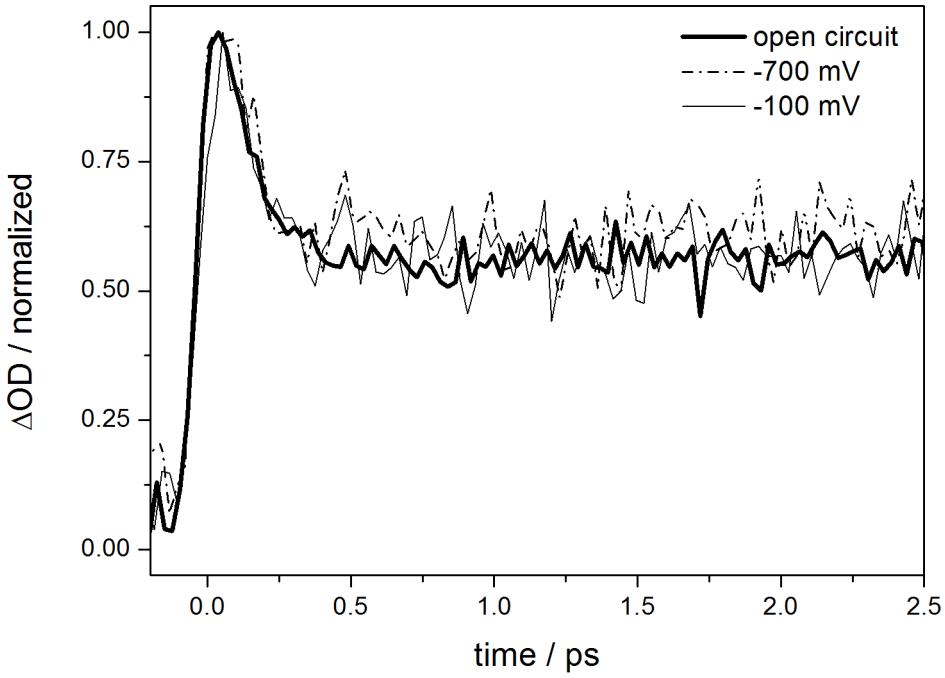


**Figure 4.15:** The ESA decay traces for a full D149/ZnO DSC under open circuit conditions (thick line) and with different applied potentials i.e -100 mV (thin line) and -700 mV (dash-dotted line).

injection times, an experiment was proposed where both pump and probe pulses could be generated in either of two NOPAs. The resulting NOPA-NOPA measurements improved temporal resolution to 40 $\pm$ 5 fs. The remarkable shot-to-shot stability of the output also resulted in improved signal-to-noise. Despite these improvements, the resulting measurements, shown in Figure 4.16, still showed no applied potential dependence of the injection signature lifetime.

This can be rationalized when considering that the conductivity of the porous ZnO electrode is quite low. The potential difference, in the order of a few hundred mV, is applied between the FTO layer of the photo-anode and the electrolyte interface, a distance in the order of $\mu$m. The potential energy barrier for an electron to cross the D149/ZnO interface, a distance on a molecular scale due to the monolayer of adsorbed dye, can thus be easily overcome. This picture may be too simple an approximation to reality, it has been stated independently that there is no space-charge-region present in the porous electrolyte-filled ZnO. The results suggest that when a counter potential is applied to the cell resulting in stagnation of the photocurrent and considering that photo-generated charge injection is unaffected, electrons will accumulate in the conduction band of the semiconductor. This is consistent with observations made on ruthenium sensitized $TiO_2$ DSCs [44].

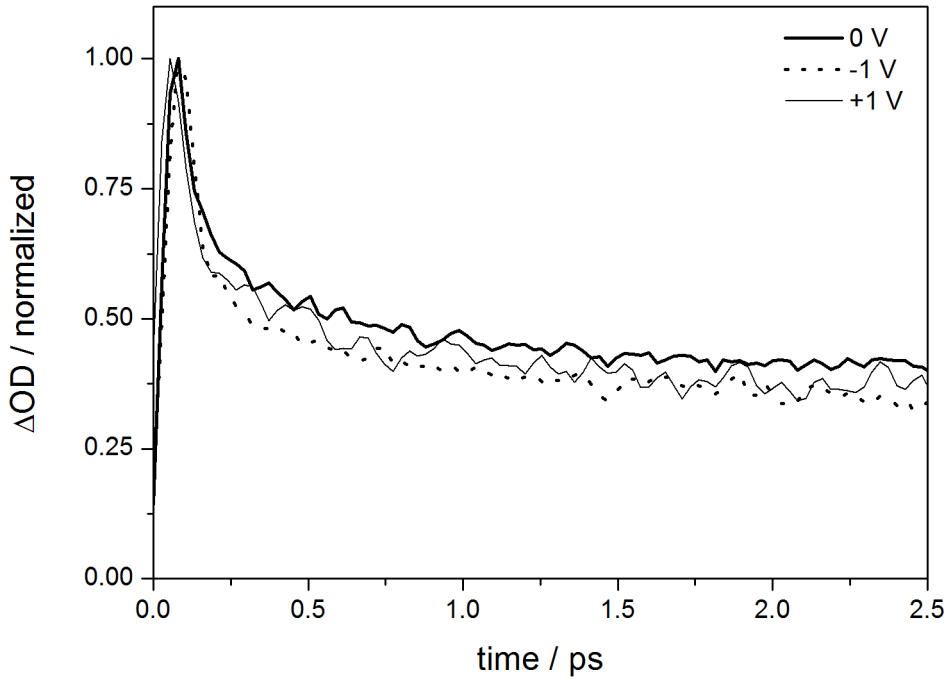


**Figure 4.16:** The ESA decay traces for a full D149/ZnO DSC with different applied potentials recorded in a NOPA-pumped, NOPA-probed setup. Measurements were done under short circuit (thick line), and under extreme bias potentials of opposite polarity i.e -1 V (dotted line) and +1 V (thin line).

## The Lithium Ion effect

Since the DSCs we were investigating showed higher $J_{SC}$ values if Li cations were added to the electrolyte as opposed to larger cations like TBA, experiments were conducted to determine whether the predicted lowering of the conduction band edge by Li ions was responsible. In Figure 4.17, the temporal evolution of the ESA signal with ultrafast decay due to charge transfer is plotted for two different cells. Both have identical D149/ZnO photo-electrodes, but are in contact with two different electrolytes. To one, 0.5 M TBAI and 0.5 M $LiClO_4$ are added, to the other 0.5 M TBAI and 0.5 M $TBAClO_4$. It should be noted that both contain 0.1 M $I_2$, which leads to formation of the redox couple when added to the solvent, which in both cases is a 4:1 volume mixture of ethylenecarbonate and acetonitrile. What becomes apparent from Figure 4.17 is that the injection seems to occur faster for the Li ion-containing sample, presumably due to improved coupling of the dye's $S_1$ state with a higher density of states in ZnO. This is consistent with the predicted consequences of a lower conduction band edge. Fits to the decay trace produced an ultrafast component below 150 fs, the measured injection time for the photo-electrode in contact with air, faster than the temporal resolution of the NOPA-pumped

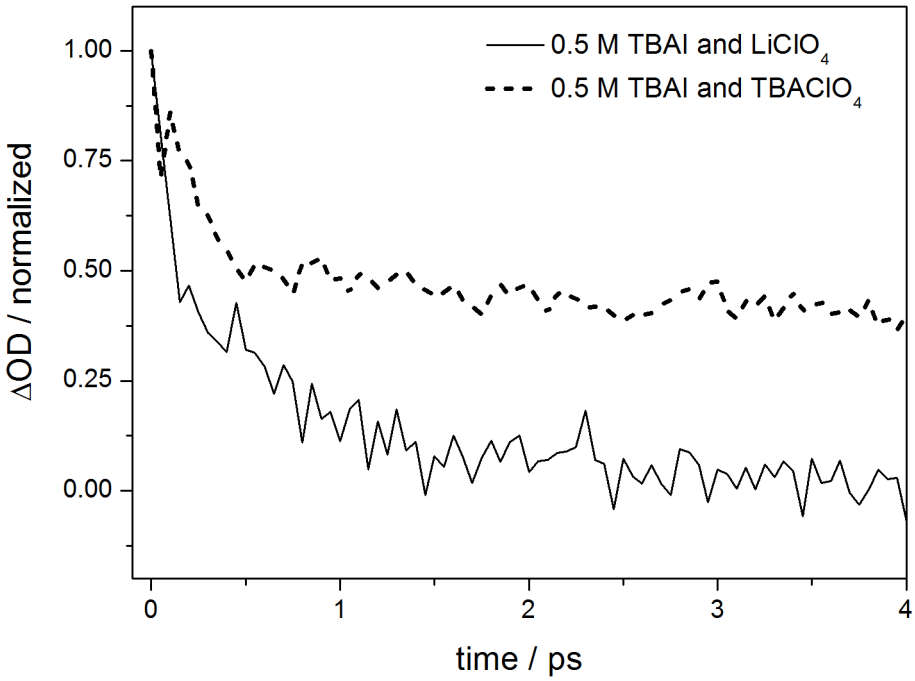


**Figure 4.17:** ESA decay trace of DSCs with electrolytes containing 0.5 M TBAI and 0.5 M $LiClO_4$ (solid line) and 0.5 M TBAI and 0.5 M $TBAClO_4$ (dashed line). The smaller Li cation accelerates electron injection by lowering the conduction band edge.

supercontinuum-probed setup. Conversely, the cell with the higher concentration of large TBAI molecules was fitted with a decay constant of 230 ± 40 fs, slower than the injection of a freestanding photo-electrode. The same phenomenon was observed in the study of Wang et al [34], already cited in the previous chapter. They noted that the electron back-reaction with $I_3^-$ was surprisingly rapid for the largest cation TBAI and that the electron diffusion length was notably reduced resulting in lower injection efficiency. Although this was measured for a ruthenium-based sensitizer on $TiO_2$, a similar mechanism may be responsible for our concurring observations.

In order to extract a lifetime for the DSC containing Li cations, a measurement was conducted on a sample containing Li cations, specifically 0.1 M LiI and 0.5 M TPAI, with the NOPA-NOPA setup described in the section on electron injection under operating conditions. The result is plotted in Figure 4.18. The decay trace of a photo-electrode exposed to air at ESA maximum is added as control measurement and confirms the electron injection time measured with the supercontinuum-probed setup. We determined the decay time of the Li cation- containing sample to be 60 ± 10 fs. We also note that in the measurements conducted on Li-containing samples in both setups, the ESA absorption maximum was blue-shifted to 620 nm. The presence of the smaller Li cations

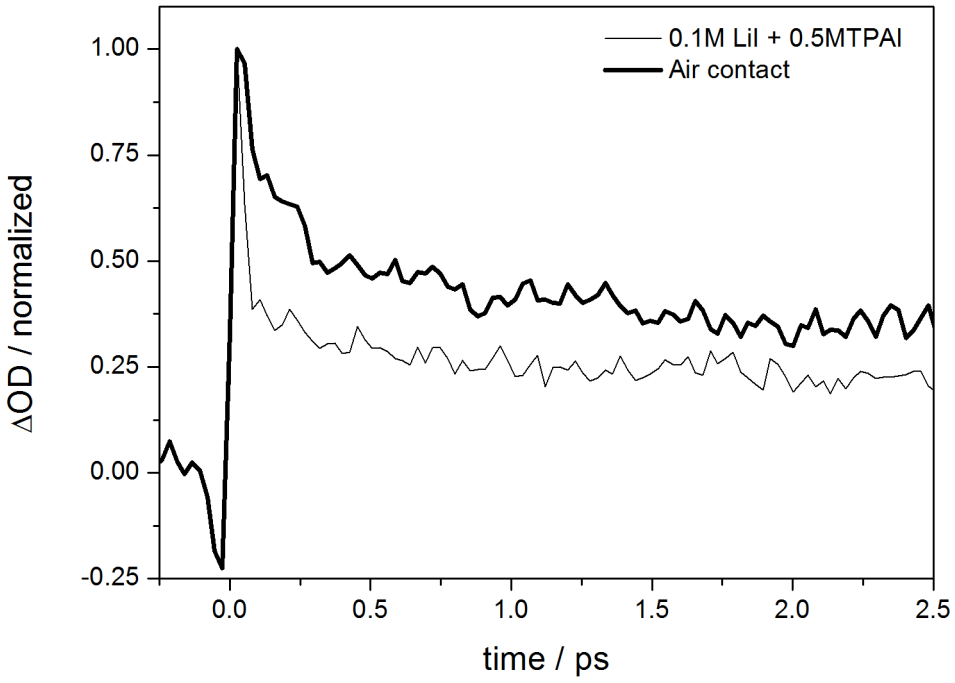


**Figure 4.18:** High resolution NOPA-NOPA measurement of ESA decay trace of a D149/ZnO photo-electrode (thick line) as reference and a DSC with electrolyte containing 0.1 M LiI and 0.5 M TPAI (thin line). The Li ion effect reduces the ESA lifetime and is fitted with an ultrafast component of 60 fs.

in the electrolytic solution may result in an enhanced response to the change in dipole moment when the dye is excited into the $S_1$ state and lower the potential energy.

## Aggregation effects

Direct comparisons of the transient photodynamics of photo-electrodes produced with and without the aid of cholic acid to prevent aggregation of D149 were made to establish whether aggregated dye molecules affected electron injection. As is evident from Figure 4.19, the electron injection occurs at the same rate for both samples. Not surprising, considering only the surface-adsorbed dye molecules are expected to inject charges into the semiconductor's conduction band. We also need to take into account that the dye-loading for samples investigated with optical techniques in transmission as is the case here, needs to be kept adequately low which may mitigate the dye's inclination to form aggregates. Nevertheless, measurements done on these samples with time-correlated single photon counting (TCSPC) by project partners on our request, did show differences in the fluorescence lifetimes. Transient spectroscopy is quite insensitive to fluorescence and is generally only detected on an intensity scale that is visible to the naked eye. TCSPC is orders of

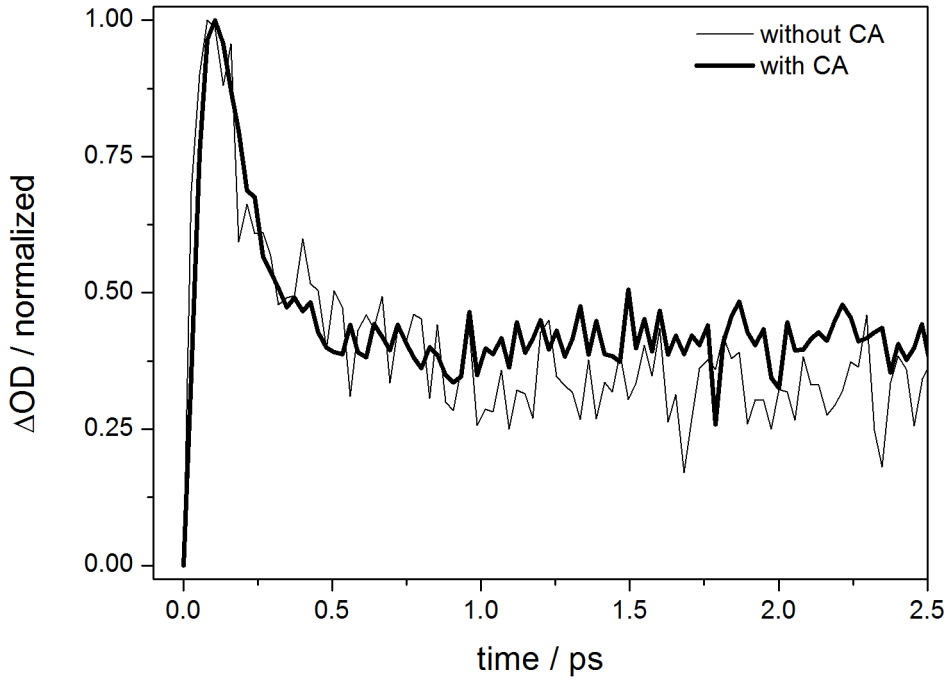


**Figure 4.19:** ESA decay traces at band maximum of 650 nm of D149/ZnO photo-electrodes produced with (solid line) and without (thin line) the use of cholic acid as co-adsorbate. No noticeable effect is observed on the primary electron injection.

magnitude more sensitive, partly due to the perpendicular arrangement of the detector and excitation pulse relative to the sample. The results, found in the appendix, show that the sample without co-adsorbate[9] fluoresces with intensity an order of magnitude greater than the sample with co-adsorbate[10]. If we take fluorescence to be an indicator of aggregate formation, the co-adsorbate prevents multilayer deposition even at low dye-loading concentrations. The discrepancy in fluorescence lifetime, shorter for the sample with co-adsorbate, is confirmation for the presence of co-adsorbate. The co-adsorbate acts as a spacer between D149 molecules within the monolayer and facilitates faster radiative deactivation

This section investigated the effects of various parameters, of interest from a technical perspective, on a complete solar cell. The primary electron injection from the excited state of the dye to the conduction band of ZnO was monitored by analyzing the decay of the ESA band maximum and was found to be independent of several parameters; incident wavelength[11], addition of a co-adsorbate that prevents dye aggregation and the application

[9] see FigureA.2
[10] see FigureA.1
[11] provided the dye absorbs and $S_1$ is populated

of a bias potential. Additionally, we noted the importance of measuring photo-electrodes under inert conditions to simplify data analysis and that electrolyte composition affects the dynamics. The implications that all of the above has for cell performance and what has been learnt as a result regarding the properties of the cell will be reviewed in the following chapter, the conclusion.

# Conclusion

Femtosecond transient absorption spectroscopy was used to characterize the photodynamics of the indoline dye D149, as used in D149/ZnO solar cells. The dye being the primary absorber in the visible wavelength region where these measurements were conducted.

As a first step, the molecule was measured in solution. After excitation along the $S_1 \leftarrow S_0$ transition at 530 nm, fluorescence and excited state absorption (ESA) was observed. These signatures along with the ground state bleaching (GSB) showed equal decay times of about 300 ps. The results implied that, in solution, the dominant decay mechanism is fluorescence.

When the dye molecule was adsorbed to a porous ZnO substrate as in the photo-electrode of a D149/ZnO dye sensitized solar cell, the fluorescence signal was absent. Additionally the ESA showed an ultrafast decay component of 150 fs, not reflected in the GSB decay trace. The emergence of absorption bands of the oxidized dye molecules confirmed that charge transfer was taking place. From the data, geminate (intramolecular) recombination of the excited dye was found to occur on a 170 ps timescale, whilst non-geminate (intermolecular) recombination of injected electrons back to the dye's ground state occurred on the timescale of several ns.

A complete D149/ZnO solar cell showed no significant changes on the fs to ps scale dynamics, but the addition of the electrolyte accelerated the decay of the absorption band of oxidized D149 to about 1 ns. It was therefore found to intercept non-geminate recombination and to effectively regenerate the ground state of the dye.

The above results are the main discussion points in a paper published by our research team [45] and are summarized by the Jablonski diagram in Figure 4.20.

The ultrafast ESA decay was used as main indicator of electron injection into ZnO and the effect of several parameters on this signature was investigated. Interestingly, in all these complete DSC samples the normalized decays of the ESA signature routinely fell to 50% - 40% of its initial absorption on the ultrafast timescale, consistent with the 60% IPCE value measured for a ZnO photo-electrode sensitized in D149 for 1 min, as per the dye-loading for the measured cells.

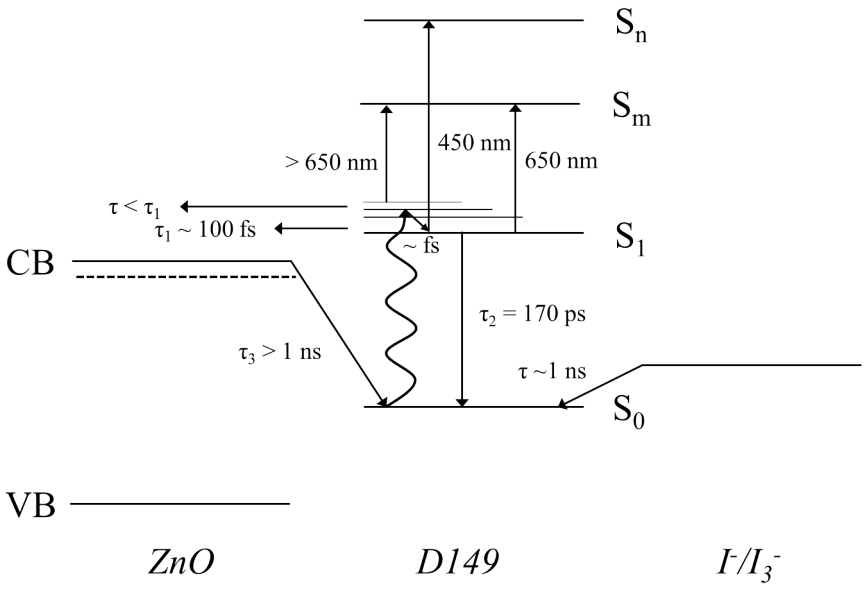


**Figure 4.20:** Jablonski diagram summarizing the characterization of D149 photodynamics in D149/ZnO DSCs that was achieved in this work.

The co-adsorbate showed that it prevented dye aggregation in time-correlated single photon counting measurements, but had no effect on the electron injection.

Applied bias potentials did not affect the electron injection despite stopping the external current. This is consistent with the view that the D149/ZnO interface (and indeed most DSC photo-electrodes) are highly porous, sponge-like structures where electrons in the conduction band of ZnO, oxidized molecules and ions in the interpenetrating electrolyte shield each other from external electric fields and charge transport occurs mainly by diffusion. Excitation with different wavelengths revealed higher injection rates for vibrationally hot excited states. Finally, the electrolyte composition was found to affect electron injection. $Li^+$, in particular was found to lower the conduction band edge, resulting in improved electron injection and higher $J_{SC}$. The lowered conduction band edge does however, imply a lower photovoltage for the cell, bringing about a trade-off scenario for the power delivered by such a DSC.

# A. Appendix

## Time-correlated single photon counting results

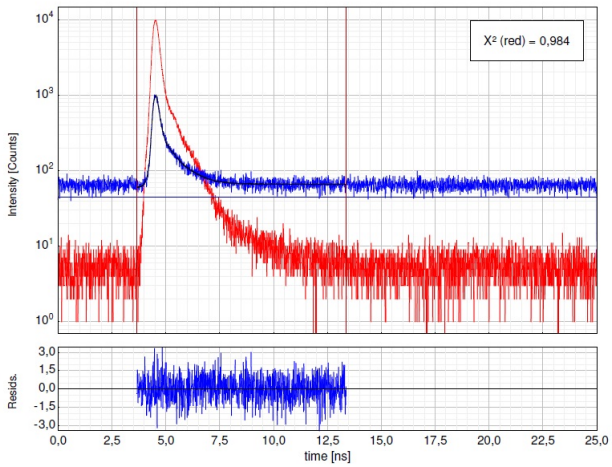


**Figure A.1:** TCSPC results for D149/ZnO DSC produced with the use of a co-adsorbate, cholic acid, to prevent dye aggregation. The top graph shows the instrument response function of the setup (red line) and the fluorescence signal (blue line). The bottom graph shows the residual of the fit to the data. The fluorescence decay is too rapid and intensity too weak for effective characterization.

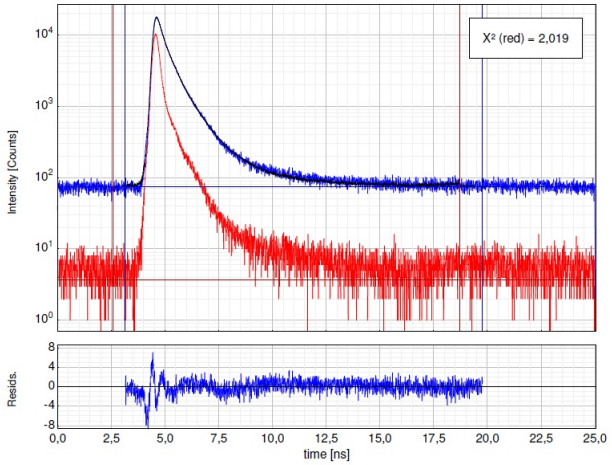


**Figure A.2:** TCSPC results for D149/ZnO DSC produced *without* the use of a co-adsorbate. Here the fluorescence decay (blue line) is larger in intensity and slower than the instrument response function (red line). When compared to the fluorescence of samples with co-adsorbate (Figure A.1) the decay is longer and the intensity greater by an order of magnitude.

# Bibliography

[1] B. O'Regan and M. Grätzel. A low-cost, high-efficiency solar cell based on dye-sensitized colloidal $TiO_2$ films. *Nature*, **353**:737–740 (1991).

[2] M. Grätzel. Recent advances in sensitized mesoscopic solar cells. *Accounts of chemical research*, **42**:1788–1798 (2009).

[3] I. Chung, B. Lee, J. He, R. P. H. Chang, and M. G. Kanatzidis. All-solid-state dye-sensitized solar cells with high efficiency. *Nature*, **485**:486–489 (2012).

[4] K. Tennakone, G. R. R. A. Kumara, A. R. Kumarasinghe, K. G. U. Wijayantha, and P. M. Sirimanne. A dye-sensitized nano-porous solid-state photovoltaic cell. *Semiconductor Science and Technology*, **10**:1689 (1995).

[5] K. Murakoshi, R. Kogure, Y. Wada, and S. Yanagida. Solid State Dye-Sensitized $TiO_2$ Solar Cell with Polypyrrole as Hole Transport Layer. *Chemistry Letters*, **26**:471–472 (1997).

[6] S. Ito, S. M. Zakeeruddin, R. Humphry-Baker, P. Liska, R. Charvet, et al. High-Efficiency Organic-Dye- Sensitized Solar Cells Controlled by Nanocrystalline-$TiO_2$ Electrode Thickness. *Advanced Materials*, **18**:1202–1205 (2006).

[7] K. Premaratne, G. Kumara, R. Rajapakse, and M. Karunarathne. Highly efficient, optically semi-transparent, ZnO-based dye-sensitized solar cells with Indoline D-358 as the dye. *Journal of Photochemistry and Photobiology A: Chemistry*, **229**:29–32 (2012).

[8] S. Higashijima, H. Miura, T. Fujita, Y. Kubota, K. Funabiki, et al. Highly efficient new indoline dye having strong electron-withdrawing group for zinc oxide dye-sensitized solar cell. *Tetrahedron*, **67**:6289–6293 (2011).

[9] S. Higashijima, Y. Inoue, H. Miura, Y. Kubota, K. Funabiki, et al. Organic dyes containing fluorene-substituted indoline core for zinc oxide dye-sensitized solar cell. *RSC Advances*, **2**:2721–2725 (2012).

[10] A. Hagfeldt and M. Grätzel. Molecular Photovoltaics. *Accounts of Chemical Research*, **33**:269–277 (2000).

[11] N. J. Cherepy, G. P. Smestad, M. Grätzel, and J. Z. Zhang. Ultrafast electron injection: implications for a photoelectrochemical cell utilizing an anthocyanin dye-sensitized $TiO_2$ nanocrystalline electrode. *The Journal of Physical Chemistry B*, **101**:9342–9351 (1997).

[12] J. B. Asbury, R. J. Ellingson, H. N. Ghosh, S. Ferrere, A. J. Nozik, et al. Femtosecond IR study of excited-state relaxation and electron-injection dynamics of $Ru(dcbpy)_2(NCS)_2$ in solution and on nanocrystalline $TiO_2$ and $Al_2O_3$ thin films. *The Journal of Physical Chemistry B*, **103**:3110–3119 (1999).

[13] J. B. Asbury, E. Hao, Y. Wang, and T. Lian. Bridge length-dependent ultrafast electron transfer from Re polypyridyl complexes to nanocrystalline $TiO_2$ thin films studied by femtosecond infrared spectroscopy. *The Journal of Physical Chemistry B*, **104**:11957–11964 (2000).

[14] R. J. Ellingson, J. B. Asbury, S. Ferrere, H. N. Ghosh, J. R. Sprague, et al. Dynamics of Electron Injection in Nanocrystalline Titanium Dioxide Films Sensitized with [Ru(4,4'-dicarboxy-2,2'-bipyridine)$_2$(NCS)$_2$] by Infrared Transient Absorption. *The Journal of Physical Chemistry B*, **102**:6455–6458 (1998).

[15] M. Fakis, E. Stathatos, G. Tsigaridas, V. Giannetas, and P. Persephonis. Femtosecond Decay and Electron Transfer Dynamics of the Organic Sensitizer D149 and Photovoltaic Performance in Quasi-Solid-State Dye-Sensitized Solar Cells. *The Journal of Physical Chemistry C*, **115**:13429–13437 (2011).

[16] A. Furube, R. Katoh, K. Hara, T. Sato, S. Murata, et al. Lithium Ion Effect on Electron Injection from a Photoexcited Coumarin Derivative into a $TiO_2$ Nanocrystalline Film Investigated by Visible-to-IR Ultrafast Spectroscopy. *The Journal of Physical Chemistry B*, **109**:16406–16414 (2005).

[17] M. A. Green, K. Emery, Y. Hishikawa, W. Warta, and E. D. Dunlop. Solar cell efficiency tables (version 39). *Progress in Photovoltaics: Research and Applications*, **20**:12–20 (2012).

[18] A. Hagfeldt, G. Boschloo, L. Sun, L. Kloo, and H. Pettersson. Dye-Sensitized Solar Cells. *Chemical Reviews*, **110**:6595–6663 (2010).

[19] I. Repins, M. A. Contreras, B. Egaas, C. DeHart, J. Scharf, et al. 19.9% efficient $ZnO/CdS/CuInGaSe_2$ solar cell with 81.2% fill factor. *Progress in Photovoltaics: Research and Applications*, **16**:235–239 (2008).

[20] C. J. Brabec. Organic photovoltaics: technology and market. *Solar Energy Materials and Solar Cells*, **83**:273 – 292 (2004).

[21] S. E. Shaheen, D. S. Ginley, and G. E. Jabbour. Organic-based photovoltaics: toward low-cost power generation. *MRS bulletin*, **30**:10–19 (2005).

[22] B. Kippelen and J.-L. Brédas. Organic photovoltaics. *Energy & Environmental Science*, **2**:251–261 (2009).

[23] J. Burschka, N. Pellet, S.-J. Moon, R. Humphry-Baker, P. Gao, et al. Sequential deposition as a route to high-performance perovskite-sensitized solar cells. *Nature*, **499**:316–319 (2013).

[24] R. A. Marcus and N. Sutin. Electron transfers in chemistry and biology. *Biochimica et Biophysica Acta (BBA)-Reviews on Bioenergetics*, **811**:265–322 (1985).

[25] A. Yella, H.-W. H.-W. Lee, H. N. Tsao, C. Yi, A. K. Chandiran, et al. Porphyrin-Sensitized Solar Cells with Cobalt (II/III)-Based Redox Electrolyte Exceed 12 Percent Efficiency. *Science*, **334**:629–634 (2011).

[26] J.-J. Cid, M. García-Iglesias, J.-H. Yum, A. Forneli, J. Albero, et al. Structure-function relationships in unsymmetrical zinc phthalocyanines for dye-sensitized solar cells. *Chem. Eur. J.*, **15**:5130–5137 (2009).

[27] Z.-S. Wang, K. Hara, Y. Dan-oh, C. Kasada, A. Shinpo, et al. Photophysical and (photo)electrochemical properties of a coumarin dye. *J. Phys. Chem. B*, **109**:3907–3914 (2005).

[28] T. Dentani, K. Nagasaka, K. Funabiki, J. Jin, T. Yoshida, et al. Flexible zinc oxide solar cells sensitized by styryl dyes. *Dyes and Pigments*, **77**:59–69 (2008).

[29] T. Yoshida, J. Zhang, D. Komatsu, S. Sawatani, H. Minoura, et al. Electrodeposition of Inorganic/Organic Hybrid Thin Films. *Advanced Functional Materials*, **19**:17–43 (2009).

[30] M. K. Nazeeruddin, A. Kay, I. Rodicio, R. Humphry-Baker, E. Müller, et al. Conversion of light to electricity by cis-X2bis(2,2'-bipyridyl-4,4'-dicarboxylate)ruthenium(II) charge-transfer sensitizers (X= Cl-, Br-, I-, CN-, and SCN-) on nanocrystalline titanium dioxide electrodes. *Journal of the American Chemical Society*, **115**:6382–6390 (1993).

[31] D. Look. Recent advances in ZnO materials and devices. *Materials Science and Engineering: B*, **80**:383–387 (2001).

[32] S. Pearton, D. Norton, K. Ip, J. Heo, and T. Steiner. Recent progress in processing and properties of ZnO. *Progress in Materials Science*, **50**:293–340 (2005).

[33] Y. Sakuragi, X.-F. Wang, H. Miura, M. Matsui, and T. Yoshida. Aggregation of indoline dyes as sensitizers for ZnO solar cells. *Journal of Photochemistry and Photobiology A: Chemistry*, **216**:1 – 7 (2010).

[34] H. Wang and L. M. Peter. Influence of Electrolyte Cations on Electron Transport and Electron Transfer in Dye-Sensitized Solar Cells. *The Journal of Physical Chemistry C*, **116**:10468–10475 (2012).

[35] R. Katoh, M. Kasuya, S. Kodate, A. Furube, N. Fuke, et al. Effects of 4-tert-Butylpyridine and Li Ions on Photoinduced Electron Injection Efficiency in Black-Dye-Sensitized Nanocrystalline $TiO_2$ Films. *The Journal of Physical Chemistry C*, **113**:20738–20744 (2009).

[36] A. El-Zohry, A. Orthaber, and B. Zietz. Isomerization and Aggregation of the Solar Cell Dye D149. *The Journal of Physical Chemistry C*, **116**:26144–26153 (2012).

[37] G. Bosman. *Transient absorption spectroscopy of metal complexes: dithizonatophenylmercury(II) and derivatives.* Ph.D. thesis, Stellenbosch University (2012).

[38] T. Le Bahers, T. Pauporté, G. Scalmani, C. Adamo, and I. Ciofini. A TD-DFT investigation of ground and excited state properties in indoline dyes used for dye-sensitized solar cells. *Physical chemistry chemical physics*, **11**:11276–84 (2009).

[39] D. R. Klug, T. Rech, D. M. Joseph, J. Barber, J. R. Durrant, et al. Primary processes in isolated Photosystem {II} reaction centres probed by magic angle transient absorption spectroscopy. *Chemical Physics*, **194**:433 – 442 (1995).

[40] P. W. Lohse, J. Kuhnt, S. I. Druzhinin, M. Scholz, M. Ekimova, et al. Ultrafast photoinduced relaxation dynamics of the indoline dye D149 in organic solvents. *Phys. Chem. Chem. Phys.*, **13**:19632–19640 (2011).

[41] A. Fattori, L. M. Peter, H. Wang, H. Miura, and F. Marken. Fast Hole Surface Conduction Observed for Indoline Sensitizer Dyes Immobilized at Fluorine-Doped Tin Oxide $TiO_2$ Surfaces. *The Journal of Physical Chemistry C*, **114**:11822–11828 (2010).

[42] U. B. Cappel, S. M. Feldt, J. Schöneboom, A. Hagfeldt, and G. Boschloo. The influence of local electric fields on photoinduced absorption in dye-sensitized solar cells. *Journal of the American Chemical Society*, **132**:9096–101 (2010).

[43] F. Willig, C. Zimmermann, S. Ramakrishna, and W. Storck. Ultrafast dynamics of light-induced electron injection from a molecular donor into the wide conduction band of a semiconductor as acceptor. *Electrochimica acta*, **45**:4565–4575 (2000).

[44] J. Teuscher, J.-D. Décoppet, A. Punzi, S. M. Zakeeruddin, J.-E. Moser, et al. Photoinduced Interfacial Electron Injection Dynamics in Dye-Sensitized Solar Cells under Photovoltaic Operating Conditions. *The Journal of Physical Chemistry Letters*, **3**:3786–3790 (2012).

[45] E. Rohwer, C. Richter, N. Heming, K. Strauch, C. Litwinski, et al. Ultrafast Photodynamics of the Indoline Dye D149 Adsorbed to Porous ZnO in Dye-Sensitized Solar Cells. *ChemPhysChem*, **14**:132–139 (2013).